scientific reports

OPEN

Synthesis of triarylpyridines with sulfonate and sulfonamide moieties via a cooperative vinylogous anomeric-based oxidation

Morteza Torabi[1], Mohammad Ali Zolfigol[1✉], Meysam Yarie[1], Behrouz Notash[2], Saeid Azizian[3] & Mina Mirzaei Azandaryani[3]

Herein, novel magnetic nanoparticles with pyridinium bridges namely Fe_3O_4@SiO_2@PCLH-TFA through a multi-step pathway were designed and synthesized. The desired catalyst and its corresponding precursors were characterized with different techniques such as Fourier transform infrared (FT-IR) spectroscopy, ^1H NMR, ^{13}C NMR, Mass spectroscopy, energy dispersive X-ray (EDX) analysis, thermogravimetric/derivative thermogravimetry (TG/DTG) analysis, scanning electron microscopy (SEM), transmission electron microscopy (TEM), and vibrating sample magnetometer (VSM). In addition, the catalytic application of the prepared catalyst in the synthesis of new series of triarylpyridines bearing sulfonate and sulfonamide moieties via a cooperative vinylogous anomeric-based oxidation was highlighted. The current trend revealed that the mentioned catalyst shows high recoverability in the reported synthesis.

With one glimpse at the literature, it can be found that urea and its derivatives have an extended domain of applications in agriculture, pharmaceuticals, petrochemicals, resin precursors, dyes and drugs[1–4]. Protein tyrosine kinases (PTKs), vascular endothelial growth factor receptor (VEGF), platelet-derived growth factor receptor (PDGFRB) and NADH oxidase are just a few of the biological applications of urea derivatives[5]. Substituted urea also act as versatile organo-catalyst in organic synthesis as they applied as acidic and basic catalysts, coupled with metals, polymer-based catalysts and supported catalysts[6]. The prevalent methods reported for the synthesis of urea derivatives are originally based on phosgene and isocyanates[3,7–20]. Recently, we have comprehensively reviewed the applications of biological urea-based catalysis in chemical processes[6].

Pyridine as the heart of heterocycle chemistry represents many pharmaceuticals and agrochemicals applications. Indeed, pyridine systems with their unique functionalities such as inhibiting HIV protease, anti-depressant, anti-inflammatory, anti-viral, anti-hypertensive, anti-oxidant, anti-fungal, anesthetics, cholagogue, pesticides, dyes-paints, treating hypotension or hypertensionare are an integral part of medicinal and biological chemistry[14–27]. In addition to the above, pyridine derivatives perform a key role in the area of catalysis. Pyridine-based catalysts have been explored as metal complex catalysis[28], chiral ligands for asymmetric catalysis[29], molecular machines such as rotaxanes and catenanes[30–32], organo-catalysis[33], polymer-based catalysts[34] and ionic liquids[35].

Particularly, triarylpyridine derivatives, a notable subset of pyridine family, are emerging as an important class of heterocyclic compounds that have many biological properties that contain anti-cancer[36], anti-depressant[3738] and anti-bacterial[38] activities. Moreover, triarylpyridines have been applied as chemosensors[39], ligands[40], and important intermediates for directional synthesis of insecticides, and surfactants[41]. Some of the synthetic routes of triarylpyridines include cyclocondensation reaction of an aldehyde, ketone and an ammonium salt as the nitrogen source[42], cyclocondensation of ketone oxime/oxime acetates with aldehydes[43] or ketone with benzyl

[1]Department of Organic Chemistry, Faculty of Chemistry, Bu-Ali Sina University, 6517838683 Hamedan, Iran. [2]Department of Inorganic Chemistry and Catalysis, Shahid Beheshti University, Evin, Tehran, Iran. [3]Department of Physical Chemistry, Faculty of Chemistry, Bu-Ali Sina University, 6517838683 Hamedan, Iran. ✉email: zolfi@basu.ac.ir
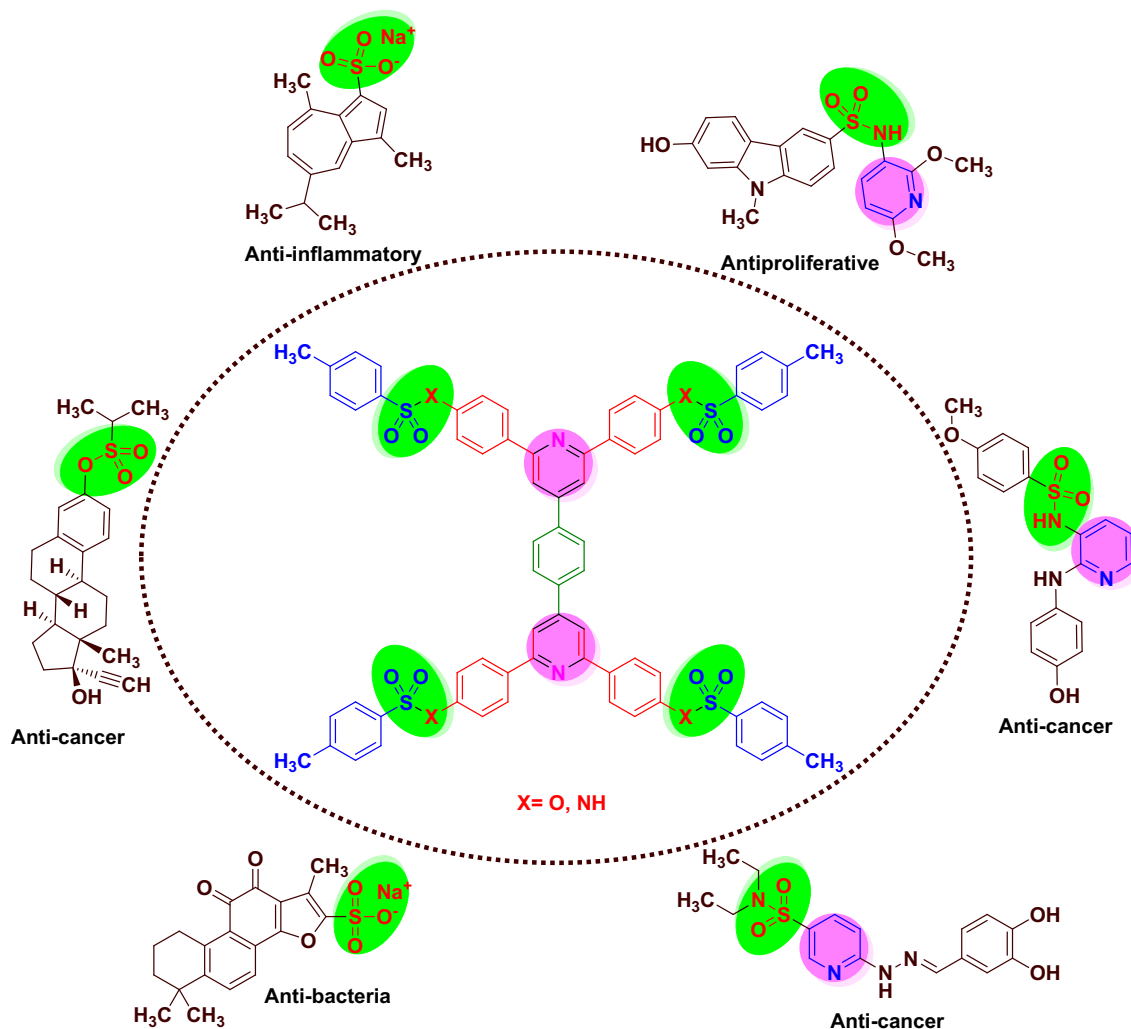
Scheme 1. Selected examples of biological applications of molecules with sulfonates and sulfonamides moieties in comparison of our investigation.

halides[44]. Nevertheless, we are trying to synthesis a new library of triarylpyridines bearing sulfonate and sulfonamide moieties.

In spite of extensive research work on magnetic nanoparticles (MNPs), they are still of interest to many scientists in various fields. The innovative rational design of organic ligands supported on heterogeneous substrates is highly promising. Immobilization of the catalytically active homogeneous species on proper heterogeneous support materials leads to formation of new catalytic systems which have the characteristics of both categories[45–50]. To a large extent, MNPs are reported as efficient supports for immobilizing homogeneous catalysts. From an economic perspective, "catalyst activity" and "catalyst separation" are vital items in modern industrial catalytic processes[51–56]. MNPs, due to high surface area compare to bulk structures, low toxicity, the capability of surface modifications and easy dispersion are dramatically very suitable for catalytic processes. Furthermore, a suitable combination of the features of MNPs and unique properties of ionic moiety can bring more benefits. Ionically tagged magnetic nanoparticles have been applied in many organic reactions[57–65].

Sulfonates are widespread in nature, and make up most of the sulfur dimension of aerobic soils. Many microorganisms can use sulfonates as a source of sulfur for growth, even when they are unable to metabolize the carbon skeleton of the compounds. Sulfonates have important pharmacological applications such as anti-oxidant, anti-inflammation and anti-apoptosis. Sometimes, it is necessary to transform drugs into their salts in order to improve physical properties such as solubility and stability. Sulfonate salts are used for this purpose. These materials are also found in many azo dyes. These compounds with different applications are reported in the literature (Scheme 1)[66–70].

Sulfonamides as the largest family of pharmaceutical compounds are frequently seen in medicinal chemistry. Sulfonamides is the first antibiotics that be used systemically and is a nice source of revolution of antibiotics in biomedicine. Many derivatives of these compounds have also been applied in agriculture. Anti-bacterial, anti-inflammatory, anti-fungal, anti-protozoal, HIV protease inhibitory, anti-Alzheimer and anti-cancer are just a small part of the medicinal applications of molecules with sulfonamide moieties. There are many reports for synthesis of sulfonamides in the literature (Scheme 1)[71–80].
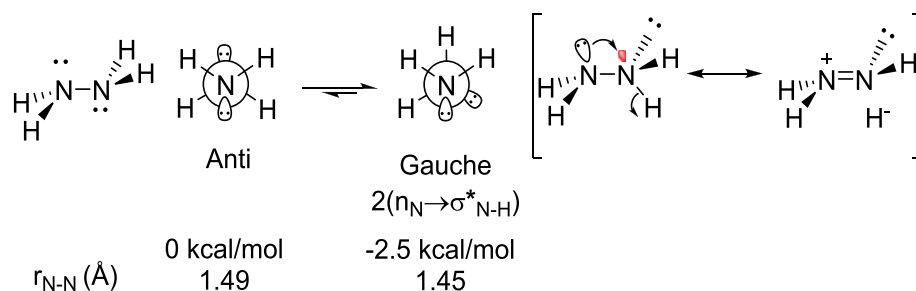
Scheme 2. The preference for gauche conformation of hydrazine originates from two $n_N \rightarrow \sigma^*_{N-H}$ stabilizing interactions.
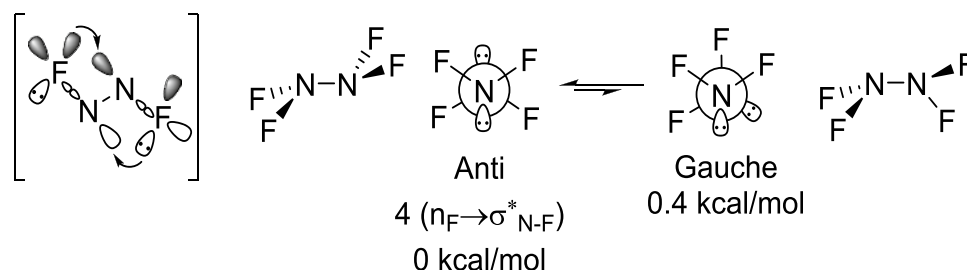
Scheme 3. Fluorination reverses the conformational preference through four $n_F \rightarrow \sigma^*_{N-F}$ stabilizing homoanomeric interactions.

In addition to the critical role of anomeric effect for the explanation of unusual observations in structure and reactivity of oxygen-containing molecules[81–85], this important stereoelectronic effect demonstrates itself as a powerful phenomenon for justifying the weird results in various heteroatom-rich compounds such as hydrazine and tetrafluorohydrazine[86–89]. In the case of hydrazine, the gauche-conformer is more stable than the anti-conformer. This observation originates from the stabilizing anomeric interactions of lone pair electrons of the nitrogen atom with a vacant antibonding orbital of adjacent N–H bond ($n_N \rightarrow \sigma^*_{N-H}$). These interactions are not possible in anti-conformer (Scheme 2). On the other hand, in the case of tetrafluorohydrazine the anti-conformer is more stable than the gauche conformation due to homoanomeric interactions. In the anti-conformer, instead of $n_N \rightarrow \sigma^*_{N-F}$ interactions, four $n_F \rightarrow \sigma^*_{N-F}$ homoanomeric interactions are operative and control the stability of conformers (Scheme 3)[90].

In the vinylogous anomeric effect, as an important subclass of anomeric effect, electron transfer interactions occurred through C=C bonds. This phenomenon has attracted the attention of many researchers[91–99]. Vinylogous anomeric effect can control the chemical reactivity. For example, Ferrier rearrangement facilitated when the leaving group exists at pseudo-axial position. In this position vinylogous anomeric effect is on and the reaction promoted by n_O-$\pi_{C=C} \rightarrow \sigma^*_{C-O}$ interaction (Scheme 4)[100].

Herein, we pursue our previous works for the synthesis of pyridines[101–107] and reported the synthesis and catalytic performance of a novel pyridinium tagged magnetic nanoparticles namely $Fe_3O_4@SiO_2@PCLH$-TFA, for the synthesis of the new library of triarylpyridines bearing sulfonate and sulfonamide moieties via a cooperative vinylogous anomeric-based oxidation mechanism[108–112] (Schemes 5, 6). We believe that the co-existence of pyridine moiety and sulfonate or sulfonamide segment within the structure of a single molecule has a significant impact on the biological importance of these versatile structures.
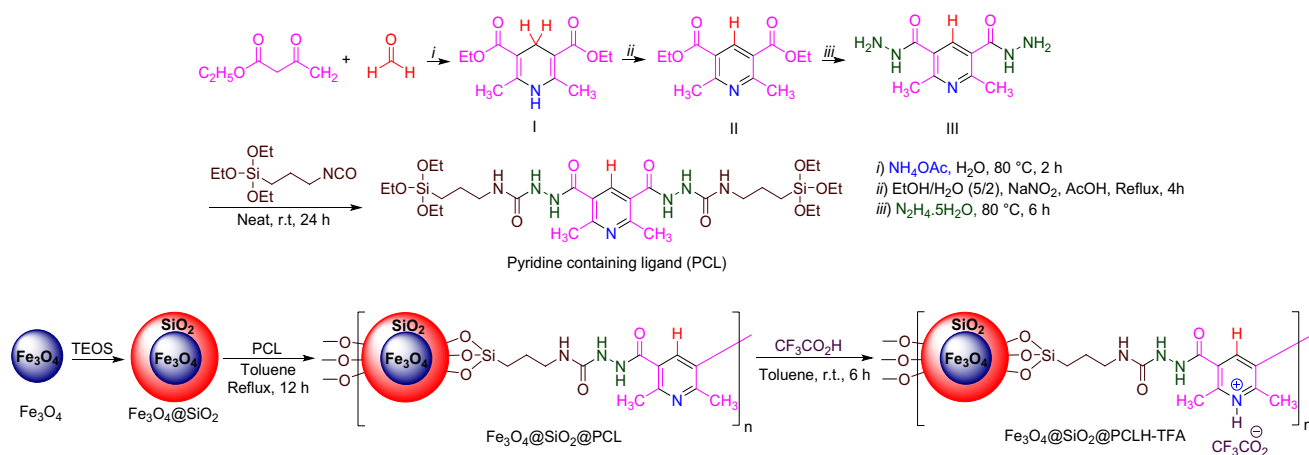
Results and discussion

Since that the pyridines with sulfonate and sulfonamide moieties have been considered as drug candidates, the synthesis of a new library of symmetrical triarylpyridines bearing sulfonate and sulfonamide moieties are our main research interest. Therefore, herein we wish to present a new catalytic system with pyridinium linkers for the synthesis of the above-mentioned compounds. According to Alabugin's theory, which has introduced stereoelectronic effects as a bridge between structure and reactivity[86–89], we have also applied the above-mentioned theory in the course of the reaction mechanism.

Divers' techniques including FT-IR, XRD, EDX, SEM, TEM, VSM and TG/DTG were employed to validate the formation of $Fe_3O_4@SiO_2@PCLH$-TFA.
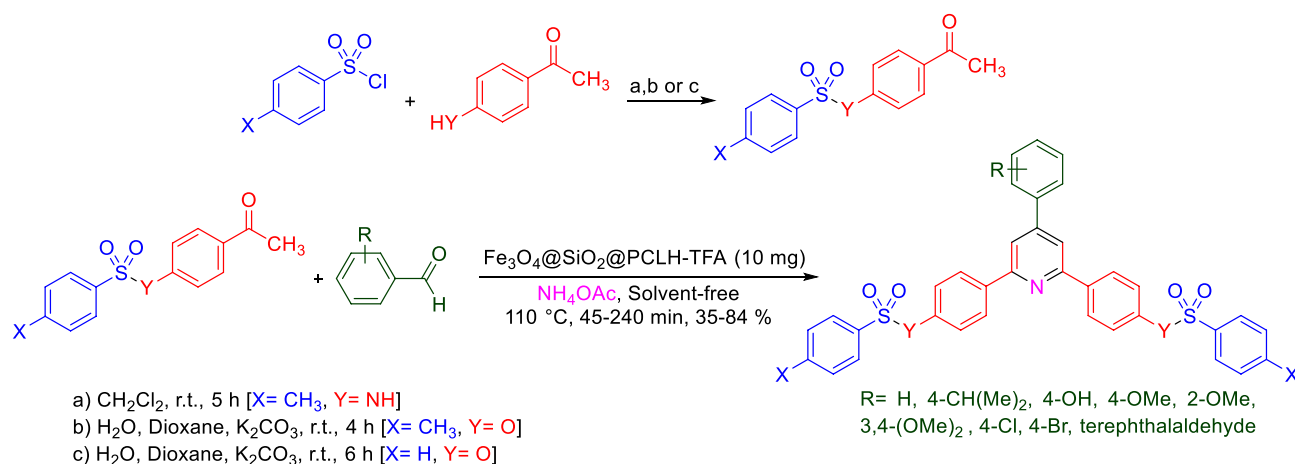
FT-IR spectrum of $Fe_3O_4@SiO_2@PCLH$-TFA and related intermediates including Fe_3O_4, $Fe_3O_4@SiO_2$, PCL and $Fe_3O_4@SiO_2@PCL$ were discussed in a comparative investigation. The changes made in each of the intermediates confirm their proper synthesis, which finally confirms the successful preparation of $Fe_3O_4@SiO_2@PCL$. The diagnostic peak of Fe_3O_4 appeared at 633 cm^{-1} is related to the stretching vibration of Fe–O. In the FT-IR spectrum of $Fe_3O_4@SiO_2$ the diagnostic peak at 1099 cm^{-1} is belonged to the Si–O–Si absorption band. The
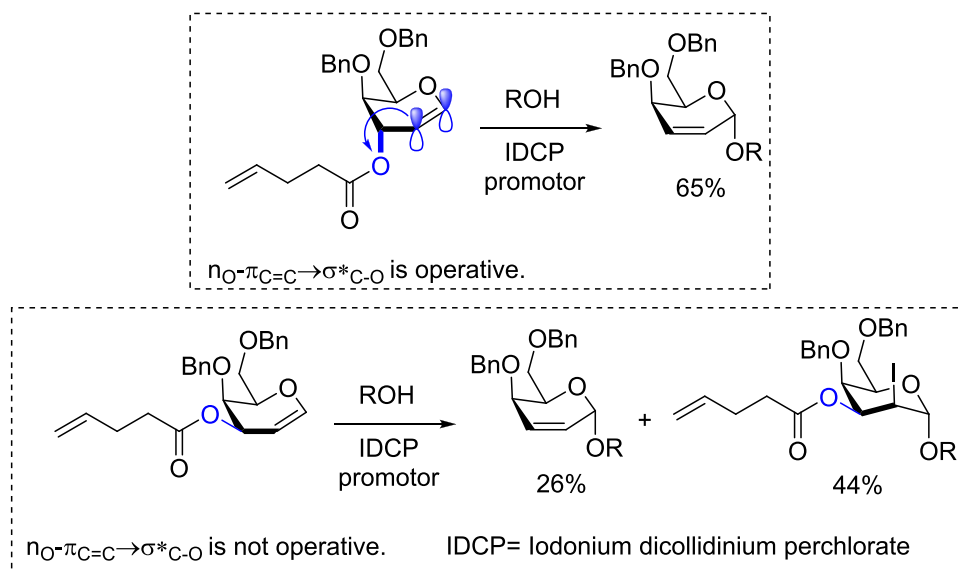
Scheme 4. The role of vinylogous anomeric effect in promotion of iodonium-catalyzed Ferrier rearrangement.

Pyridine containing ligand (PCL)

i) NH₄OAc, H₂O, 80 °C, 2 h
ii) EtOH/H₂O (5/2), NaNO₂, AcOH, Reflux, 4h
iii) N₂H₄.5H₂O, 80 °C, 6 h

Scheme 5. General experimental procedure for the targeted synthesis of Fe₃O₄@SiO₂@PCLH-TFA.

a) CH₂Cl₂, r.t., 5 h [X= CH₃, Y= NH]
b) H₂O, Dioxane, K₂CO₃, r.t., 4 h [X= CH₃, Y= O]
c) H₂O, Dioxane, K₂CO₃, r.t., 6 h [X= H, Y= O]

R= H, 4-CH(Me)₂, 4-OH, 4-OMe, 2-OMe, 3,4-(OMe)₂ , 4-Cl, 4-Br, terephthalaldehyde

Scheme 6. Synthesis of a new library of triarylpyridines bearing sulfonate and sulfonamide moieties in the presence of Fe₃O₄@SiO₂@PCLH-TFA.
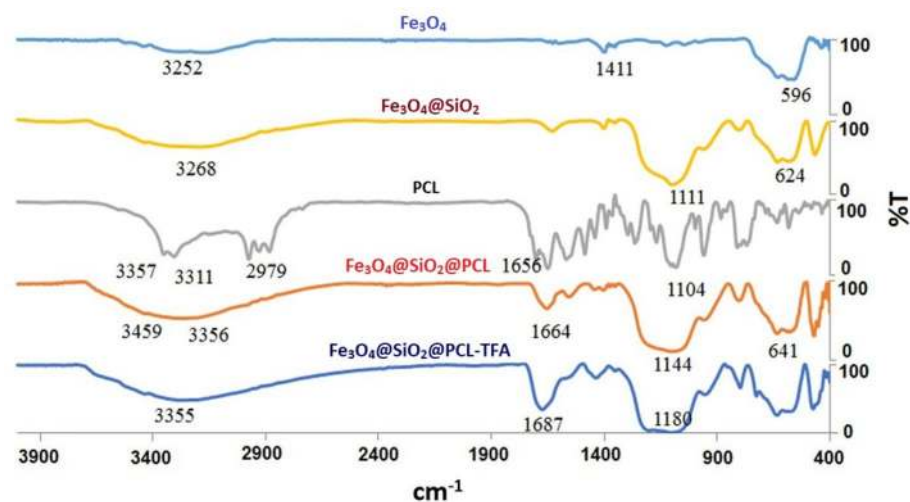
Figure 1. Comparative investigation of Fe₃O₄@SiO₂@PCLH-TFA and its corresponding intermediates.

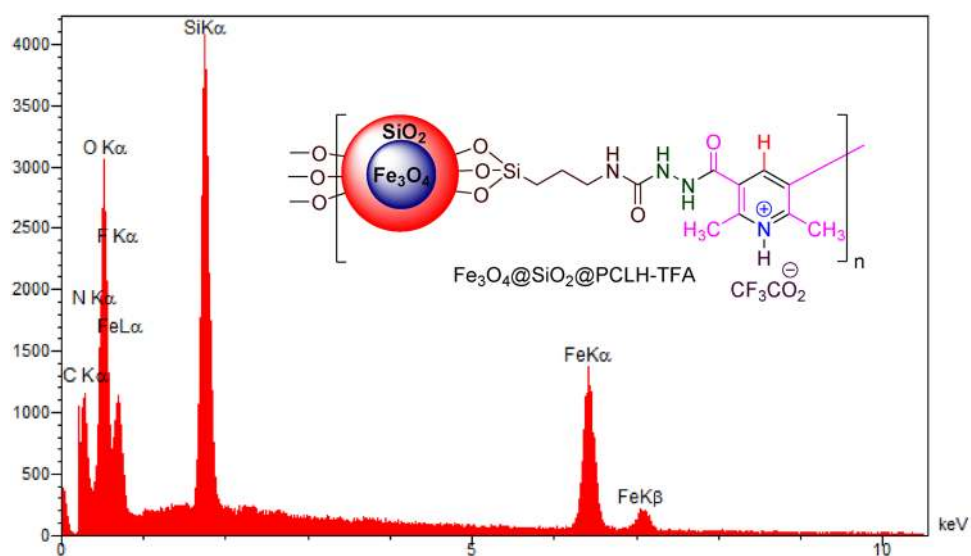**Figure 2.** EDX analysis of Fe₃O₄@SiO₂@PCLH-TFA.

carbonyl groups related to the structure of the prepared catalyst appeared at around 1687 cm^{-1} as a broad peak. In the structure of desired catalyst, the broad peak at about 2500–3500 cm^{-1} is related to pyridinium moiety, amidic NH groups of the PCL and free hydroxyl groups of the Fe₃O₄@SiO₂@PCLH-TFA (Fig. 1).

The elemental composition of Fe₃O₄@SiO₂@PCLH-TFA was characterized using energy-dispersive X-ray spectroscopy (EDX). According to the outcome data, all expected elements including iron, silicon, oxygen, carbon, nitrogen and fluorine were approved (Fig. 2). Furthermore, to confirm this observation, elemental mapping analysis was investigated (Fig. 3). The elemental mapping reveals uniform distribution of the mentioned elements.

For a better description of catalyst, the surface and morphology property analysis of Fe₃O₄@SiO₂@PCLH-TFA was also studied by SEM images. According to the SEM images the morphology of the catalyst is spherical (Fig. 4). But by more focusing, it can be seen that each sphere is made from the aggregate of smaller size nanoparticles. For further clarification, the TEM images were recorded (Fig. 5) and it clearly shows that the bigger particles are made from nanopraticles (4–6 nm) and with core–shell structure. The TEM results confirmed the obtained data from SEM images (Fig. 5).

TG has been generally applied to evaluate thermal degradation behaviour of magnetic nanoparticles. To determine the thermal behaviour of the Fe₃O₄@SiO₂@PCLH-TFA, TG/DTG was carried out. The obtained results are illustrated in Fig. 6 and show good thermal stability for the prepared Fe₃O₄@SiO₂@PCLH-TFA.

The VSM analysis was employed to determine magnetic properties of Fe₃O₄@SiO₂@PCLH-TFA in comparison with its related precursors such as Fe₃O₄ and Fe₃O₄@SiO₂. Decreasing the magnetic property of Fe₃O₄@SiO₂@PCLH-TFA compared to its precursors, indicates the successful addition of organic moieties onto the surface

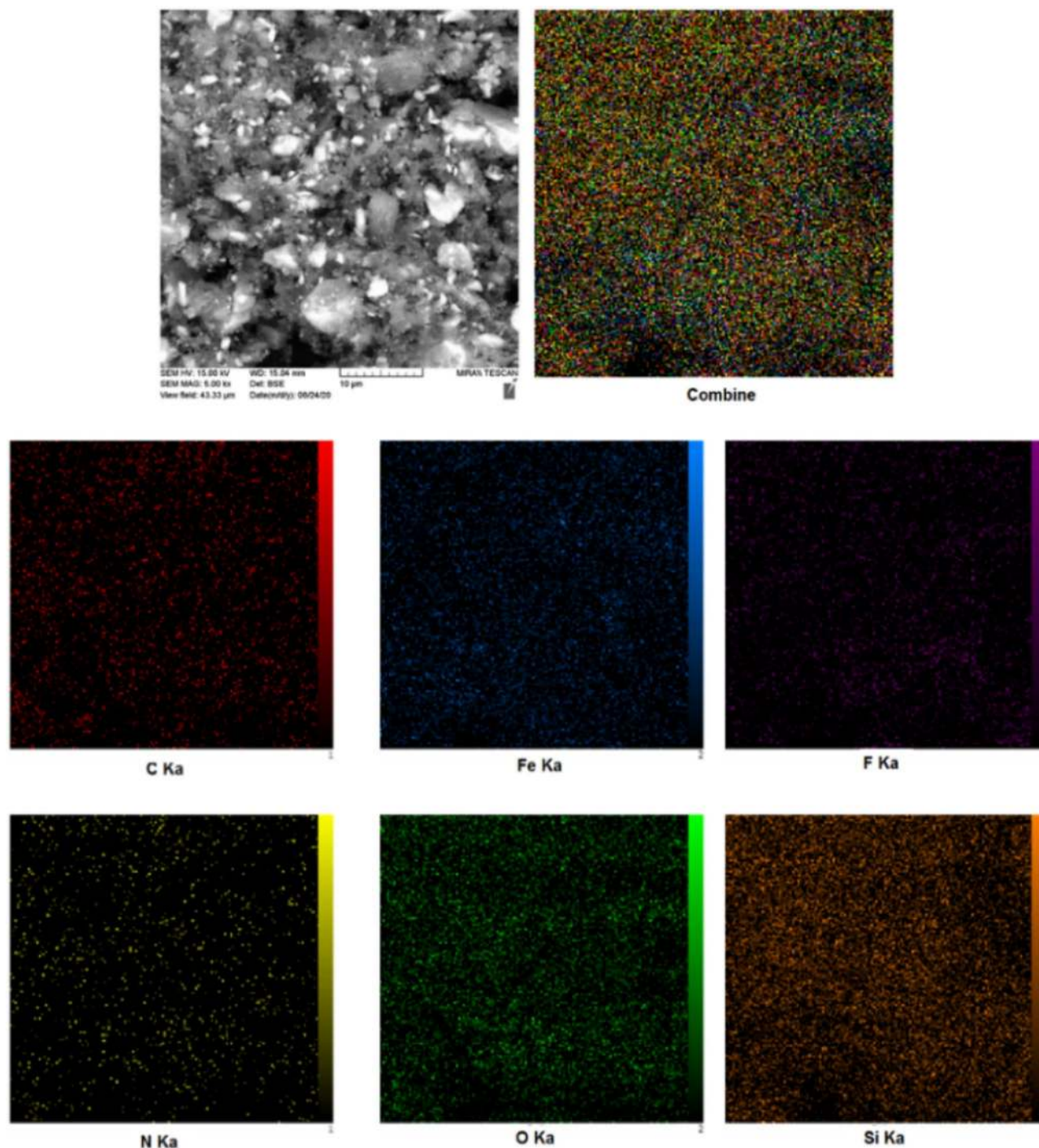**Figure 3.** Elemental mapping analysis of Fe$_3$O$_4$@SiO$_2$@PCLH-TFA.

of magnetic precursor (Fig. 7). The value of magnetic saturation of Fe$_3$O$_4$@SiO$_2$@PCLH-TFA is about 25 emu/g which is enough for its easy separation from the reaction mixture upon completion of the catalytic reaction.

After targeted and multi-step synthesis and characterization of Fe$_3$O$_4$@SiO$_2$@PCLH-TFA as a novel pyridinium tagged magnetic nanoparticles, we evaluated its catalytic performance for the synthesis of a new library of triarylpyridines bearing sulfonate and sulfonamide moieties via a cooperative vinylogous anomeric-based oxidation mechanism. For this purpose, we designed a model reaction for achieving the best operational reaction conditions. In this regard, the reaction of 4-choloro benzaldehyde, 4-acetylphenyl-4-methylbenzenesulfonate and ammonium acetate was selected and the role of solvents, temperature and amount of Fe$_3$O$_4$@SiO$_2$@PCLH-TFA as catalyst was investigated. Based on resulted experimental data, the utilization of 10 mg of Fe$_3$O$_4$@SiO$_2$@PCLH-TFA at 110 °C under solvent-free conditions is the best conditions for the synthesis of target molecules **1f.** from time and yield perspective (Table 1).
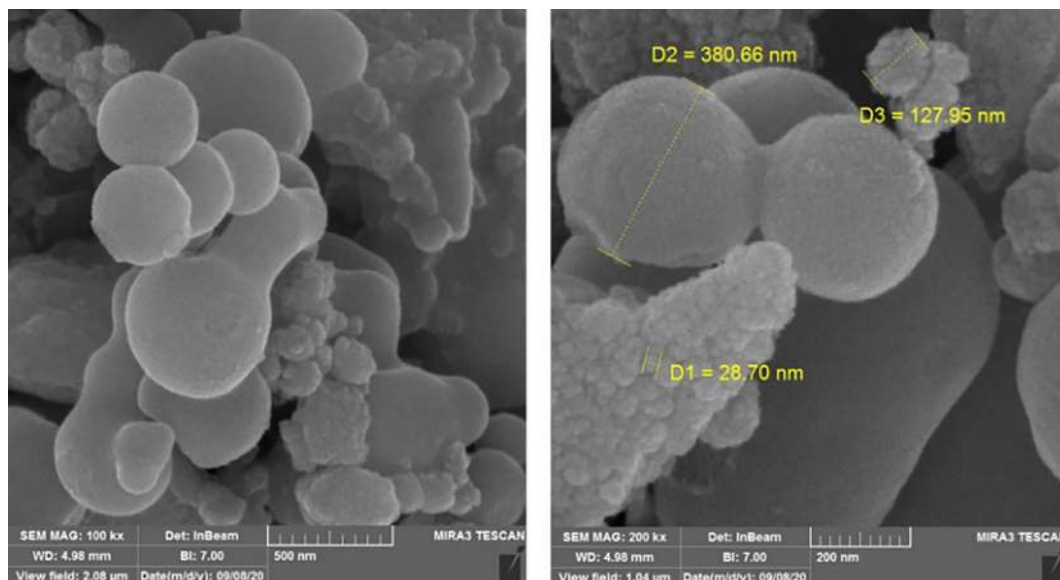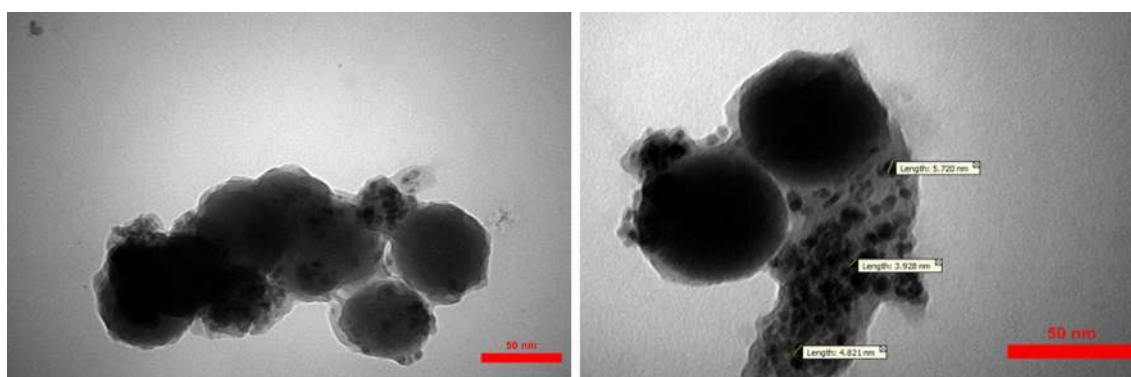
Figure 4. SEM images of Fe$_3$O$_4$@SiO$_2$@PCLH-TFA.

Figure 5. TEM images of Fe$_3$O$_4$@SiO$_2$@PCLH-TFA.

Also, we tested the model reaction (synthesis of molecule **1f.**) in the presence of related intermediates of Fe$_3$O$_4$@SiO$_2$@PCL and some known catalysts to validate the importance of the existence of ionic tag (pyridinium site) within the structure of Fe$_3$O$_4$@SiO$_2$@PCLH-TFA as the catalyst. As inserted in Table 2, the novel synthesized catalyst shows the best results in comparison with some other catalysts and verified the crucial role of the acidic and hydrogen-bond sites within the structure of the catalyst.

In another study with considering the above-mentioned encouraging results under optimal reaction conditions, we generalized a catalytic procedure for the synthesis of a new library of triarylpyridines bearing sulfonate and sulfonamide moieties using Fe$_3$O$_4$@SiO$_2$@PCLH-TFA as a novel recoverable catalyst. In this synthetic procedure, different ketones with sulfonate and sulfonamide moieties and various aromatic aldehydes bearing electron-withdrawing and electron-releasing substituents were utilized. Also, terephthaldehyde revealed promising results. The collected data are inserted in Table 3.

Also, a plausible mechanism for the synthesis of **2c** (Scheme 7) is suggested. At the first, 4-acetylphenyl-4-methylbenzenesulfonate was activated by Fe$_3$O$_4$@SiO$_2$@PCLH-TFA, and converted to its corresponding enolic form. Then the mentioned enolic form was reacted with activated benzaldehyde with catalyst. This reaction leads to the formation of chalcone intermediate **A**. Then, intermediate **A** undergoes a nucleophilic attack from the enolic form of 4-acetylphenyl-4-methylbenzenesulfonate which resulted in the formation of intermediate **B**. In the next step, ammonia derived from the dissociation of ammonium acetate attacked to intermediate **B** and enamine **C** is produced. After this, through a sequential reaction including, a tautomerization process, intramolecular nucleophilic attack and dehydration, intermediate **C** converted to intermediate **E**. Finally, releasing of molecular H$_2$ is facilitated based on a cooperative vinylogous anomeric-based oxidation (CVABO) in intermediate **E** which leads to the formation of the desired molecule after deprotonation of intermediate **F**.

Considering the high potential of magnetic catalysts in recovering and reusing processes, we investigated the recovering and reusing of Fe$_3$O$_4$@SiO$_2$@PCLH-TFA in a model reaction for the synthesis of target molecule **1f.** under optimal reaction conditions (Fig. 8). After completing each run of reaction, the catalyst was separated from the mixture of reaction using an external magnet. Then, the separated catalyst was washed several times
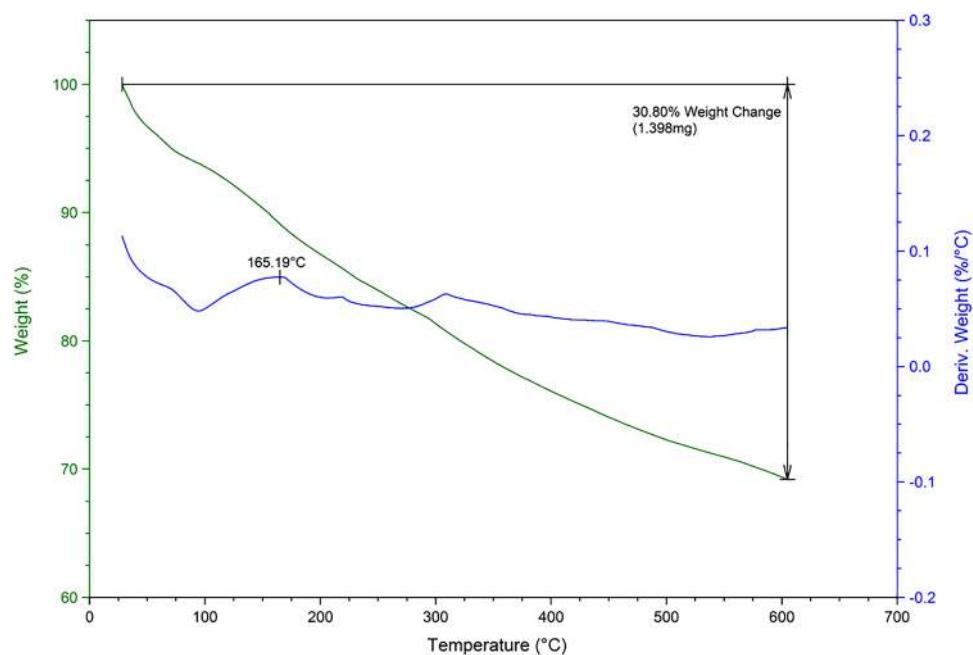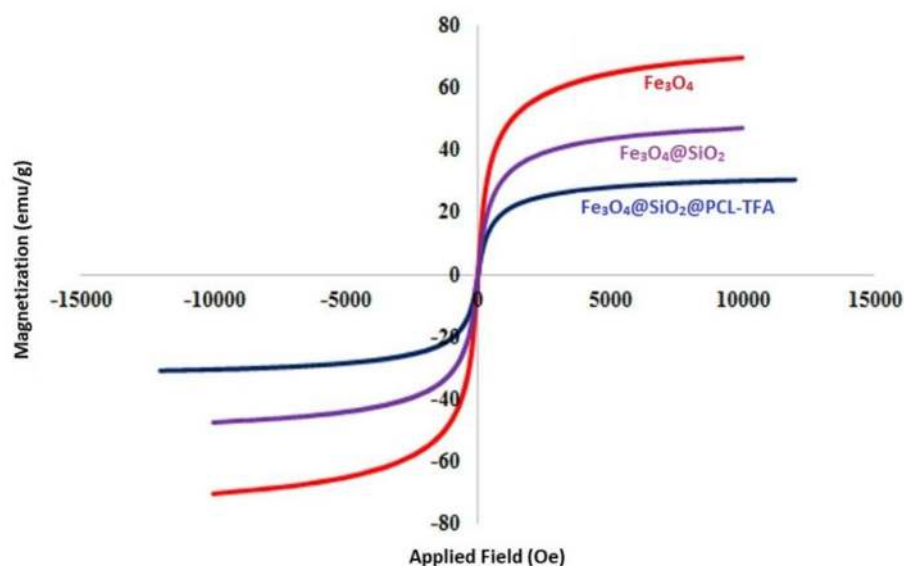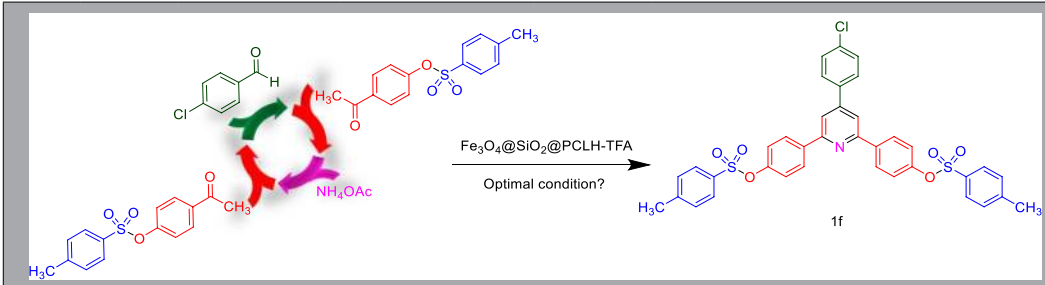
Figure 6. TG/DTG curve of Fe$_3$O$_4$@SiO$_2$@PCLH-TFA.

Figure 7. VSM curves of Fe$_3$O$_4$@SiO$_2$@PCLH-TFA in comparison with its related magnetic precursors.

with ethanol and dried. This process was performed seven times without significant reduction in the reaction efficiency. Finally, the stability of the catalyst was confirmed by comparison of FT-IR spectra of recovered and fresh catalyst (See ESI).

In a separate study, the reaction kinetics was investigated by UV–visible spectroscopy upon the model reaction for the synthesis of molecule 1f. For this purpose, the UV–visible spectrum of reaction components was recorded as a function of time. At different time intervals, a sample of the reaction mixture was dissolved in ethanol and its spectrum was recorded with a UV–visible spectrophotometer. The obtained spectrums at different time intervals were presented in Fig. 9a. The peak centered at 250 nm doesn't show any regular variation because of the overlapping of reactants, intermediates, and products peaks. But the peak centered at about 210 nm, decreases with time, as shown by an arrow. This peak belongs to reactants since decreases with reaction time. The plot of normalized absorbance (A/A_0) at $\lambda_{max} = 210$ nm versus time is shown in Fig. 9b. This plot clearly shows non-linear decrease of absorbance versus time. The slope of this plot (rate of reaction) at $t < 20$ min is higher than its slope at $t > 20$ min, indicating higher rate of reaction at the first 20 min of reaction. At a longer time, the rate of reaction decreases.

Entry	Solvent	Temperature (°C)	Catalyst loading (mg)	Time (min.)	Yield (%)[a]
1	–	120	10	45	80
2	–	110	20	45	84
3[b]	–	**110**	**10**	**45**	**84**
4		110	5	60	74
5	–	110	–	45	Trace
6	–	110	–	120	40
7	–	100	10	60	72
8	–	90	10	70	55
9	–	80	10	70	40
10	–	70	10	90	Trace
11	H_2O	Reflux	10	180	–
12	EtOH	Reflux	10	180	Trace
13	*n*-Hexane	Reflux	10	180	–
14	EtOAc	Reflux	10	180	–
15	CH_2Cl_2	Reflux	10	180	–

Table 1. Optimizing of the reaction condition for the synthesis of **1f**. Reaction conditions: 4-cholorobenzaldehyde (1 mmol, 0.140 g), 4-acetylphenyl-4-methylbenzenesulfonate (2 mmol, 0.580 g), and ammonium acetate (1.5 mmol, 0.115 g). [a]Related to isolated yields. [b]Data for the model reaction under air, and inert atmosphere (nitrogen and argon) are similar.

Entry	Catalyst	Load of catalyst	Yield (%)
1	Fe_3O_4	10 mg	30
2	$Fe_3O_4@SiO_2$	10 mg	25
3	PCL	10 mol%	45
4	$Fe_3O_4@SiO_2@PCL$	10 mg	58
5	$Fe_3O_4@SiO_2@PCLH$-TFA	10 mg	84
6	Trifluoroacetic acid	10 mol%	55
7	*p*-Toluenesulfonic acid	10 mol%	80
8	$FeCl_3$	10 mol%	33
9	Trityl chloride	10 mol%	Trace
10	H_2SO_4	10 mol%	Trace
11	NH_2SO_3H	10 mol%	65
12	$Fe(HSO_4)_3$	10 mol%	52
13	$Al(HSO_4)_3$	10 mol%	36
14	$Ca(HSO_4)_2$	10 mol%	44
15	Silica sulfuric acid[113]	10 mg	71

Table 2. Investigation of catalytic behavior of $Fe_3O_4@SiO_2@PCLH$-TFA and its relative intermediates and some known catalysts upon the synthesis of 1f. Reaction conditions: 4-Cholorobenzaldehyde (1 mmol, 0.140 g), 4-acetylphenyl-4-methylbenzenesulfonate (2 mmol, 0.580 g), and ammonium acetate (1.5 mmol, 0.115 g), solvent-free, 110 °C, 45 min.
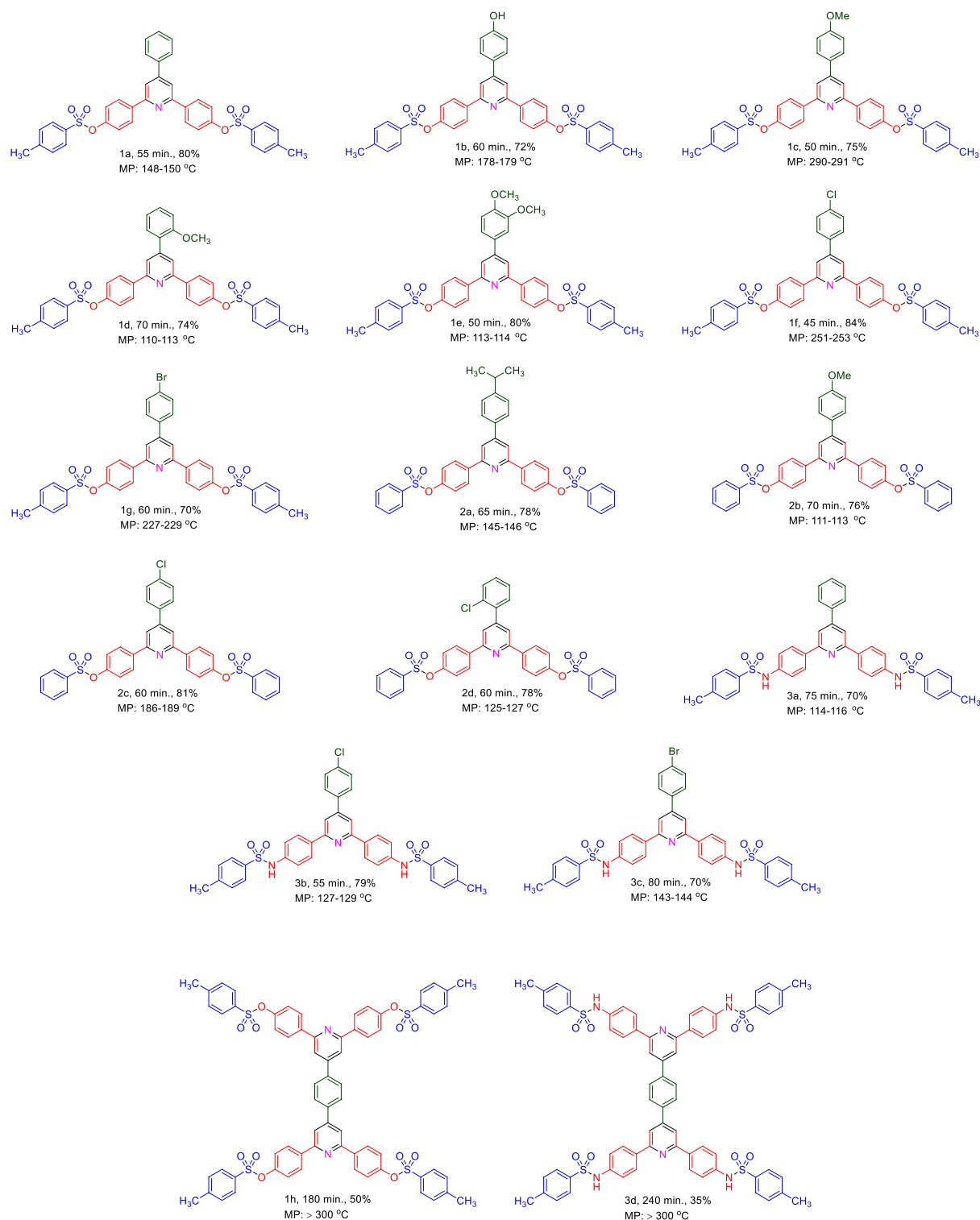
Table 3. Synthesis a new library of triarylpyridine derivatives bearing sulfonate and sulfonamide moieties in the presence of Fe$_3$O$_4$@SiO$_2$@PCLH-TFA. Reaction conditions: aldehyde (1 mmol), methyl ketone (2 mmol) and ammonium acetate (1.5 mmol, 0.115 g), Solvent-free, 110 °C, catalyst = 10 mg, reported yields are referred to isolated yields.

Also, in another investigation and similar to the synthetic protocol of PCL, we tried to use (**I**) directly for the preparation of a new dihydropyridine containing ligand (DHPCL) as a reductant reagent such as biological NADH2/NAD$^+$ systems which capable to be heterogeneous. For this goal, (**I**) and hydrazine hydrate subjected to the reaction under refluxing EtOH. Our prediction was the production of molecule (**IV**). The achieved NMR
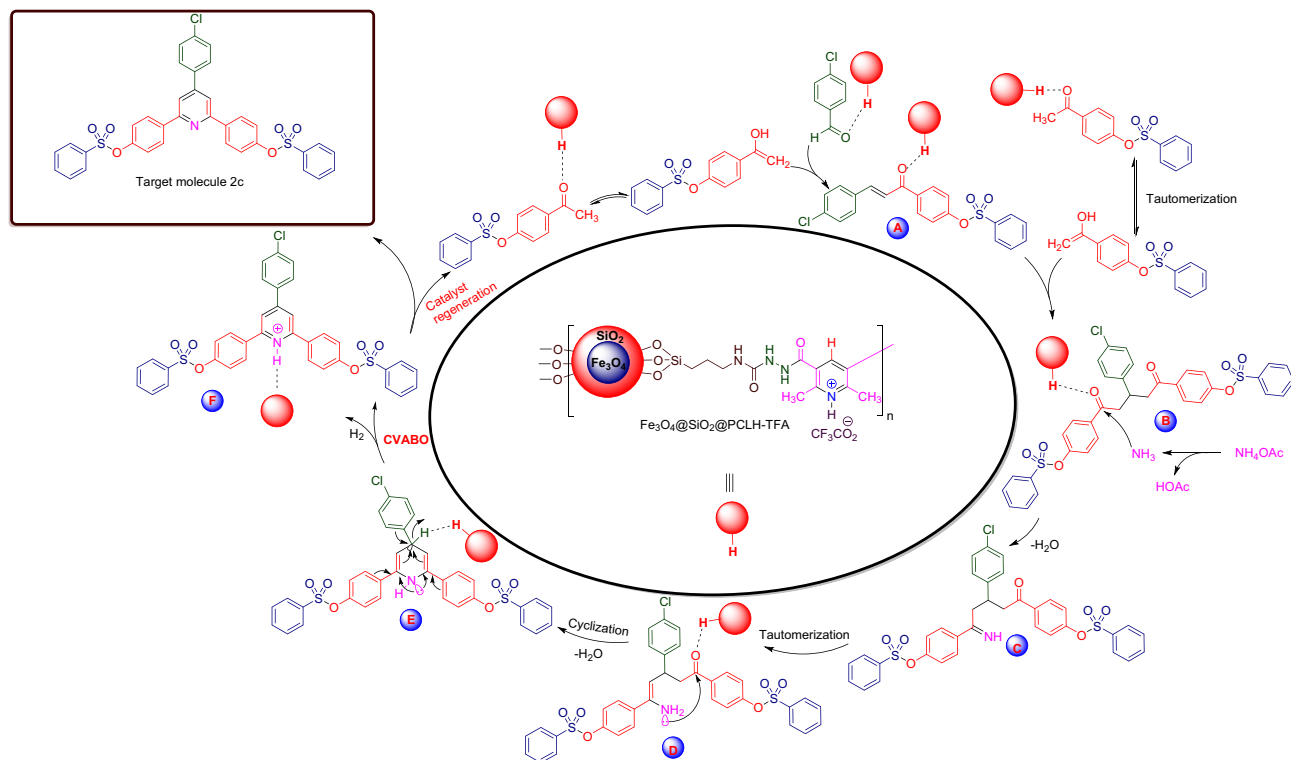
Scheme 7. A suggested plausible mechanism for the synthesis of **2c** using Fe₃O₄@SiO₂@PCLH-TFA as catalyst.

Run	1	2	3	4	5	6	7	8
Isolated yield (%)	84	84	82	81	80	77	75	71
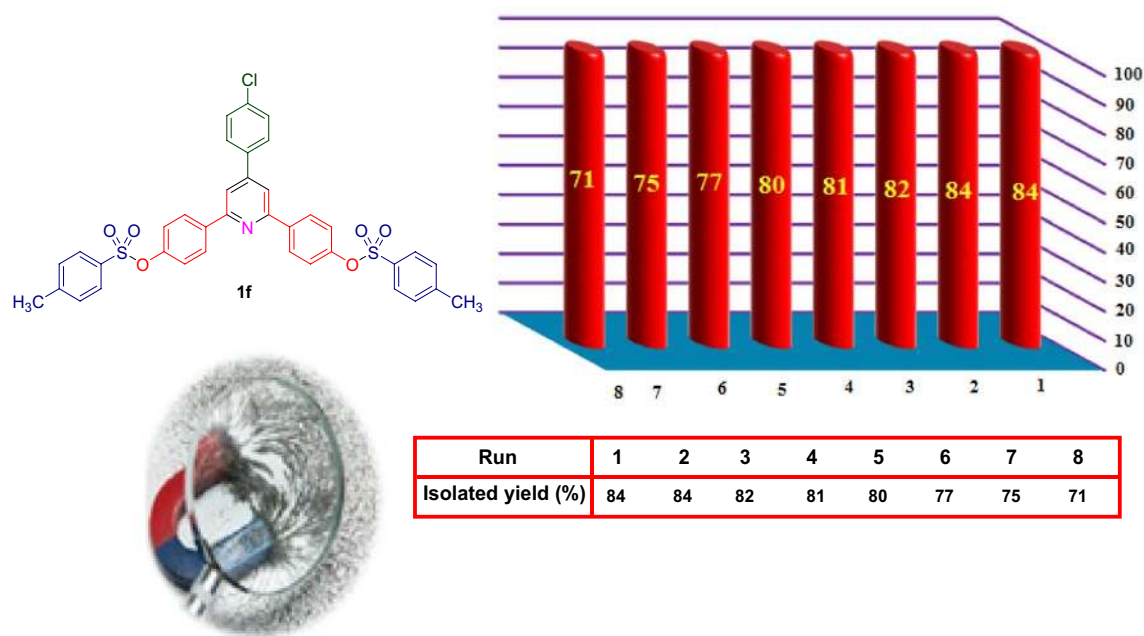
Figure 8. Recovering and reusing test of Fe₃O₄@SiO₂@PCLH-TFA upon the synthesis of **1f**.

data (see ESI) did not match the expected structure (**IV**). Initial interpretations of the obtained NMR data were apparently in accordance with a molecular cage (**V**). So, with this hypothesis, we applied X-ray crystallography to determine the exact structure. Surprisingly, based on the results of X-ray crystallography, it is revealed that 4,4′-methylenebis(5-methyl-*1H*-pyrazol-3-ol) (**VI**) has been formed (Scheme 8 and Fig. 10)[114,115]. Our literature surveys showed that the molecule (**VI**) had been previously reported[116]. A suggested plausible mechanism for the synthesis of the molecule (**VI**) is depicted in Scheme 9.

Figure 9. The reaction kinetics by using UV–Visible spectroscopy.

Scheme 8. Reaction of the **I** and hydrazine hydrate leads to formation of **VI**.

Experimental section

General. All materials and reagents were purchased from Merck and Sigma-Aldrich companies and were used without further purification. Double distilled water was used in all reactions. ^{1}H NMR spectra were recorded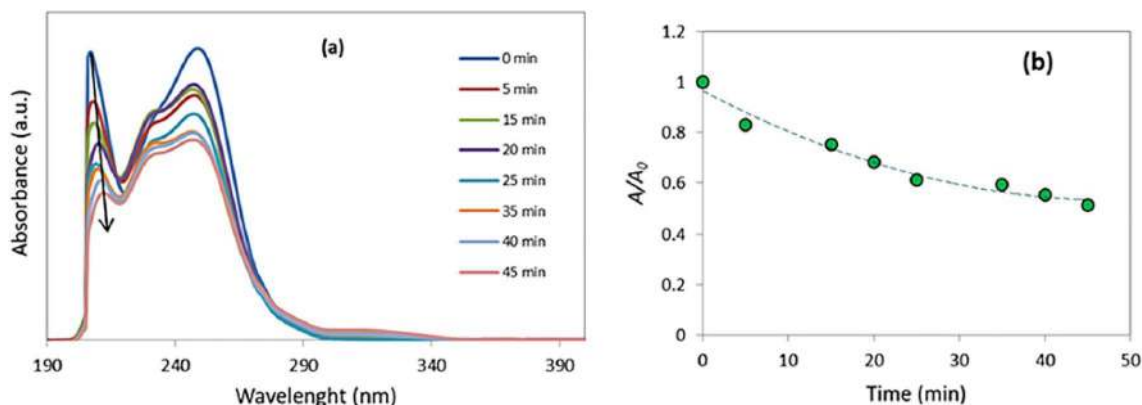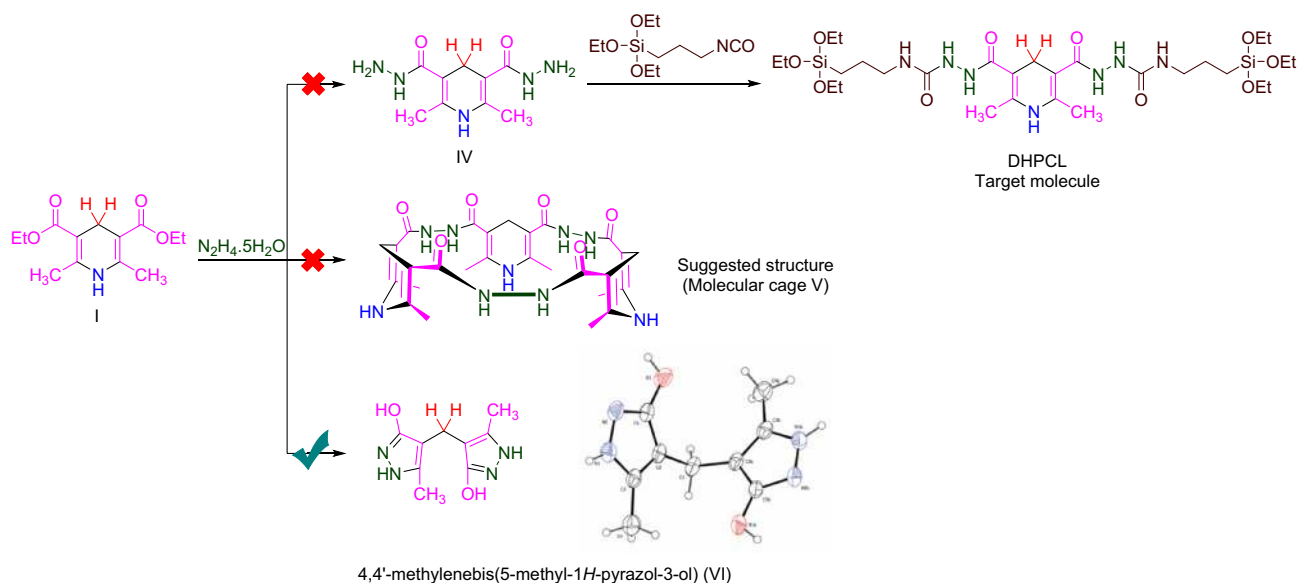 on a Bruker spectrometer operating at 300 MHz, and ^{13}C NMR spectra were recorded on a Bruker spectrometer operating at 75 MHz. TEM analysis was performed with an instrument model EM10C-100 kV from ZEISS. SEM analysis was performed with SIGMA VP instrument from ZEISS. The instrument of EDX-Mapping analysis is related to Oxford Instruments company. TGA/DTG analysis was performed under nitrogen conditions applying STA-1500 instrument from Rheometric Scientific. The magnetic properties of the catalyst were investigated with VSM analysis that was performed using LBKFB instrument from Meghnatis Daghigh Kavir Company. XRD analysis was performed with X' Pert Pro instrument from Panalytical. A UV–visible spectrophotometer (PG-Instrument- T80) was applied for the study of reaction kinetics.

General procedure for the preparation of 2,6-dimethylpyridine-3,5-dicarbohydrazide. Initially, diethyl 2,6-dimethyl-1,4-dihydropyridine-3,5-dicarboxylate (**I**) was prepared according to the previously reported procedure[117]. Then, (**I**) (20 mmol, 5.06 g) and sodium nitrite (40 mmol, 2.76 g) were dissolved in 70 mL of ethanol/water (5/2, V/V) and heated in 50 °C for 5 min. Then, acetic acid (42 mmol, 2.4 mL) was added dropwise to the reaction mixture and was refluxed for 2 h. After completing the reaction and removal of solvent, the precipitate was washed with water to give diethyl 2,6-dimethylpyridine-3,5-dicarboxylate (**II**) as a white solid in 90% yield. MP (°C) = 72–74[118]. In the next step, hydrazine hydrate (40 mmol, 4.88 g) was added to (**II**) (10 mmol, 2.51 g) and was heated for 6 h at 80 °C. After removal of water, the remained precipitate was washed with ethanol several times to give pure 2,6-dimethylpyridine-3,5-dicarbohydrazide (**III**) as a white solid.

General procedure for the synthesis of PCL. PCL was synthesized by the reaction of triethoxy(3-isocyanatopropyl) silane (5 mmol, 1.237 g) and **III** (12 mmol, 2.68 g) under neat conditions at room temperature for 24 h.
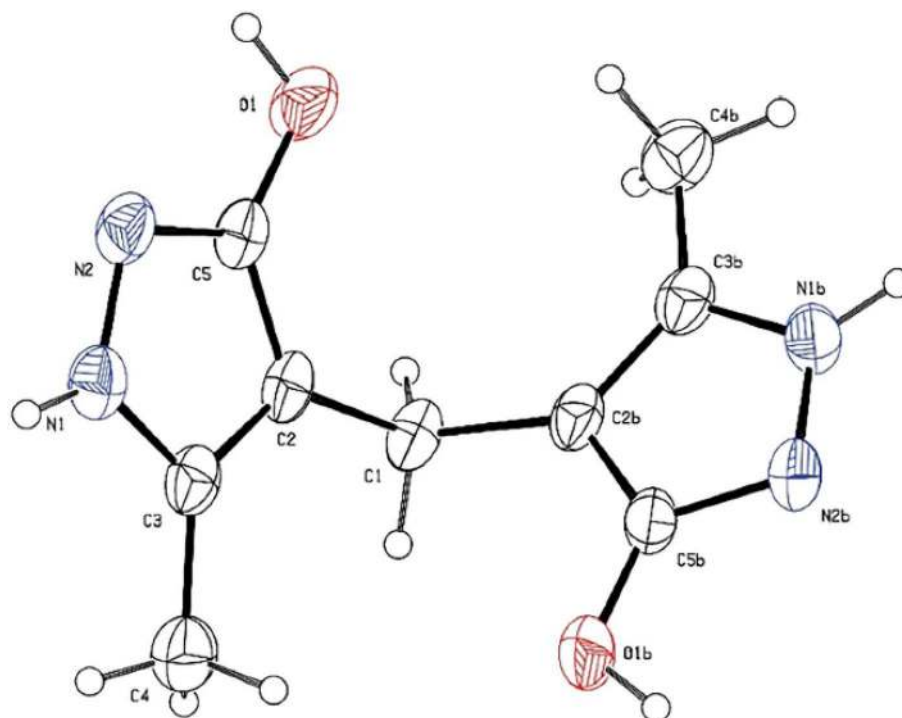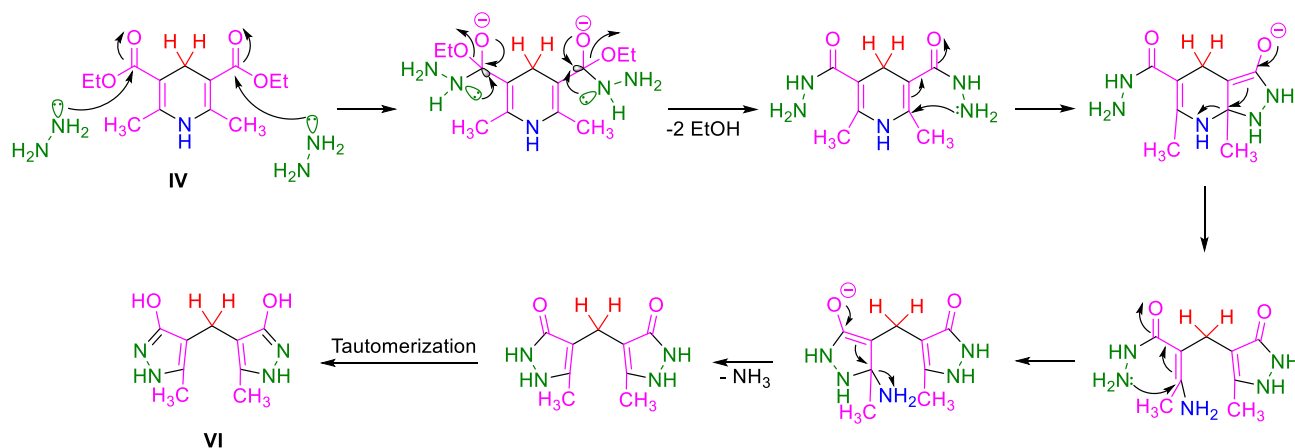
Figure 10. The ORTEP diagram of **VI**. Thermal ellipsoids are at 30% probability level. Disordered DMSO molecule has been omitted for clarity.

Scheme 9. Plausible mechanistic route to VI.

Afterward, the obtained white precipitate was washed with the mixture of ethyl acetate/chloroform (8×2 ml). The remained white precipitate was dried and characterized by FT-IR, ^{1}H NMR and ^{13}C NMR.

General procedure for the synthesis of Fe$_3$O$_4$@SiO$_2$@PCLH-TFA. At first, Fe$_3$O$_4$ nanoparticles were prepared by the same method as reported in previously reported procedure[119]. Then, 2 g of Fe$_3$O$_4$ and 3 ml ammonia and 4 ml TEOS was added to 200 ml of EtOH/H$_2$O (4/1, V/V) and stirred at room temperature for 24 h. Then, nanoparticles of Fe$_3$O$_4$@SiO$_2$ were separated by an external magnet and were washed several times with water and ethanol and finally air dried. In the next step, the prepared Fe$_3$O$_4$@SiO$_2$ (1 g) was functionalized by the reaction with ligand PCL (2 mmol, 1.38 g) under refluxing toluene at 110 °C for 12 h to give Fe$_3$O$_4$@SiO$_2$@PCL. At the final step, Fe$_3$O$_4$@SiO$_2$@PCL was treated with trifluoroacetic acid (2 mmol, 0.228 g) in toluene at room temperature for 6 h and after that, the resulted Fe$_3$O$_4$@SiO$_2$@PCLH-TFA was washed with *n*-hexane (3×30 ml) and air dried.

General procedure for the synthesis of new library of triarylpyridines bearing sulfonate and sulfonamide moieties in the presence of Fe$_3$O$_4$@SiO$_2$@PCLH-TFA. To a mixture of aldehyde derivatives (1 mmol), methyl ketones with sulfonate and sulfonamide moieties[120,121] (2 mmol) and ammonium acetate (1.5 mmol, 0.115 g), 10 mg

of Fe$_3$O$_4$@SiO$_2$@PCLH-TFA as catalyst were added. Then, the reaction mixture was stirred under solvent-free conditions at 110 °C for requisite times (Table 3). The progress of the reaction was inspected by TLC techniques (n-hexane/ethylacetate as eluent). After completion of each reaction, the reaction mixture was dissolved in hot ethanol and the insoluble nanomagnetic catalyst was isolated from the reaction mixture by using an external magnet. Then, target molecules were purified by TLC plate with n-hexane/ethyl acetate as eluent.

Spectral data.   *2,6-Dimethylpyridine-3,5-dicarbohydrazide (III).*   M.p. = 230–232 °C, FT-IR (KBr, ν, cm^{-1}): 3302, 3202, 3067, 1640, 1594, 1185. ^{1}H NMR (301 MHz, DMSO) δppm 9.54 (s, 2H, NH), 7.65 (s, 1H, Aromatic), 4.57 (s, 4H, NH$_2$), 2.54 (s, 6H, CH$_3$). ^{13}C NMR (76 MHz, DMSO) δ 167.2, 156.6, 135.2, 127.6, 23.0.

2,2′-(2,6-Dimethylpyridine-3,5-dicarbonyl)bis(N-(3-(triethoxysilyl)propyl)hydrazine-1-carboxamide) (PCL).   M.p. = 170–171 °C, FT-IR (KBr, ν, cm^{-1}): 3304, 2974, 1701, 1650, 1567, 1083. ^{1}H NMR (301 MHz, DMSO) δppm 9.89 (s, 2H, NH), 7.94–7.91 (m, 3H, Aromatic and NH), 6.49 (s, 2H, NH), 3.77 (q, 12H, J = 6 Hz, CH$_2$), 3.03 (q, 4H, J = 6 Hz, CH$_2$), 2.58 (s, 6H, CH$_3$), 1.48 (q, 4H, J = 6 Hz, CH$_2$), 1.17 (t, 18H, J = 6 Hz, CH$_3$), 0.56 (t, 4H, J = 9 Hz, CH$_2$). ^{13}C NMR (76 MHz, DMSO) δ 167.7, 158.5, 157.2, 135.6, 127.1, 58.2, 42.5, 23.9, 23.1, 18.7, 7.7.

4-Acetylphenyl benzenesulfonate.   M.p. = 60–62 °C, FT-IR (KBr, ν, cm^{-1}): 3063, 1692, 1680, 1593, 1352, 1201. ^{1}H NMR (301 MHz, DMSO) δ 8.00–7.97 (m, 2H), 7.93 -7.90 (m, 2H), 7.85–7.82 (m, 1H), 7.72–7.69 (m, 2H), 7.22–7.19 (m, 2H), 2.56 (s, 3H).

4-Acetylphenyl-4-methylbenzenesulfonate.   M.p. = 70–72 °C, FT-IR (KBr, ν, cm^{-1}): 6072, 2918, 1682, 1596, 1379, 1176. ^{1}H NMR (301 MHz, DMSO) δ 8.00–7.95 (m, 2H), 7.79 (d, J = 9 Hz, 2H), 7.47 (d, J = 9 Hz, 2H), 7.22–7.17 (m, 2H), 2.55 (s, 3H), 2.40 (s, 3H). ^{13}C NMR (76 MHz, DMSO) δ 197.1, 152.7, 146.5, 136.0, 131.7, 130.8, 130.7, 128.9, 122.7, 27.1, 21.6.

(4-Phenylpyridine-2,6-diyl)bis(4,1-phenylene)bis(4-methylbenzenesulfonate) (1a).   M.p. = 148–150 °C, FT-IR (KBr, ν, cm^{-1}): 3068, 1600, 1499, 1453, 1179. ^{1}H NMR (301 MHz, DMSO) δppm 8.34 (d, 4H, J = 9 Hz), 8.20 (s, 2H), 8.03 (dd, J = 8.0, 3 Hz, 2H), 7.82 (d, J = 9 Hz, 4H), 7.57–7.49 (m, 6H), 7.19 (d, J = 9 Hz, 4H), 2.44 (s, 6H, CH$_3$). ^{13}C NMR (76 MHz, DMSO) δ 155.6, 150.3, 150.2, 146.4, 138.1, 137.79, 131.9, 130.8, 129.9, 129.5, 129.1, 128.8, 127.9, 122.8, 117.5, 21.7.

(4-(4-Hydroxyphenyl)pyridine-2,6-diyl)bis(4,1-phenylene)bis(4-methylbenzenesulfonate) (1b).   M.p. = 178–179 °C, FT-IR (KBr, ν, cm^{-1}): 3471, 3058, 1603, 1502, 1372, 1176. ^{1}H NMR (301 MHz, DMSO) δppm 8.35 (d, 4H, J = 9 Hz), 8.24 (s, 2H), 8.05 (q, J = 9 Hz, 2H), 7.83–7.76 (m, 6H), 7.53–7.50 (m, 6H), 7.20–7.17 (m, 4H), 2.45 (s, 6H, CH$_3$). ^{13}C NMR (76 MHz, DMSO) δ 155.7, 150.4, 146.4, 138.0, 137.0, 132.4, 131.9, 130.8, 130.0, 129.2, 128.8, 128.7, 123.1, 122.8, 117.3, 21.7.

(4-(4-Methoxyphenyl)pyridine-2,6-diyl)bis(4,1-phenylene)bis(4-methylbenzenesulfonate) (1c).   M.p. = 290–291 °C, FT-IR (KBr, ν, cm^{-1}): 2923, 1603, 1501, 1368, 1153, ^{1}H NMR (301 MHz, DMSO) δ 8.32 (d, J = 9 Hz, 4H), 8.15 (s, 2H), 8.02 (d, J = 9 Hz, 2H), 7.82 (d, J = 9 Hz, 4H), 7.51 (d, J = 9 Hz, 4H), 7.18 (d, J = 9 Hz, 4H), 7.11 (d, J = 9 Hz, 2H), 3.86 (s, 3H, OCH$_3$), 2.44 (s, 6H). ^{13}C NMR (76 MHz, DMSO) δ 161.0, 155.5, 150.3, 149.7, 146.4, 138.2, 131.9, 130.8, 129.9, 129.2, 129.1, 128.8, 122.7, 116.7, 114.9, 55.8, 21.7.

(4-(2-Methoxyphenyl)pyridine-2,6-diyl)bis(4,1-phenylene)bis(4-methylbenzenesulfonate) (1d).   M.p. = 178–179 °C, FT-IR (KBr, ν, cm^{-1}): 3061, 2926, 1601, 1500, 1372, 1152. ^{1}H NMR (301 MHz, DMSO) δ 8.24 (d, J = 9 Hz, 4H), 7.99 (s, 2H), 7.81 (d, J = 9 Hz, 4H), 7.55 (dd, J = 7.5, 1.7 Hz, 1H), 7.49 (m, 5H), 7.21–7.14 (m, 6H), 3.82 (s, 3H, OCH$_3$), 2.42 (s, 6H). ^{13}C NMR (76 MHz, DMSO) δ 156.9, 154.8, 150.2, 148.8, 146.4, 138.2, 131.9, 131.0, 130.8, 129.0, 128.7, 127.5, 122.8, 121.4, 120.3, 112.4, 56.2, 21.6. ESI–MS (m/z) = calcd. for C$_{38}$H$_{31}$NO$_7$S$_2$ (M$^+$) 677.15, found: 678.

(4-(3,4-Dimethoxyphenyl)pyridine-2,6-diyl)bis(4,1-phenylene)bis(4-methylbenzenesulfonate) (1e).   M.p. = 113–114 °C, FT-IR (KBr, ν, cm^{-1}): 3064, 2923, 1600, 1501, 1370, 1263, 1152. ^{1}H NMR (301 MHz, DMSO) δ 8.33 (d, J = 9 Hz, 4H), 8.16 (s, 2H), 7.82 (d, J = 9 Hz, 4H), 7.62–7.55 (m, 2H), 7.50 (d, J = 9 Hz, 4H), 7.19 (d, J = 9 Hz, 4H), 7.11 (d, J = 9 Hz, 1H), 3.93 (s, 3H, OCH$_3$), 3.85 (s, 3H, OCH$_3$), 2.43 (s, 6H). ^{13}C NMR (76 MHz, DMSO) δ 155.4, 150.6, 150.3, 150.2, 149.7, 146.4, 138.2, 131.9, 130.8, 130.3, 129.1, 128.8, 122.7, 120.5, 117.0, 112.4, 111.3, 56.4, 56.1, 21.7. ESI–MS (m/z) = calcd. for C$_{39}$H$_{33}$NO$_8$S$_2$ (M$^+$) 707.16, found: 708.

(4-(4-Chlorophenyl)pyridine-2,6-diyl)bis(4,1-phenylene)bis(4-methylbenzenesulfonate) (1f.).   M.p. = 251–253 °C, FT-IR (KBr, ν, cm^{-1}): 3233, 1637, 1615, 1372, 1152. ^{1}H NMR (301 MHz, DMSO) δ 8.35 (d, J = 9 Hz, 4H), 8.24 (s, 2H), 8.15–8.08 (m, 2H), 7.82 (d, J = 9 Hz, 4H), 7.64 (d, J = 9 Hz, 2H), 7.52 (d, J = 9 Hz, 4H), 7.20 (d, J = 9 Hz, 4H), 2.45 (s, 6H, CH$_3$). ^{13}C NMR (76 MHz, DMSO) δ 162.8, 155.7, 150.3, 146.4, 138.0, 136.8, 136.6, 131.9, 130.8, 129.7, 129.5, 129.2, 128.8, 122.8, 117.4, 21.7.

(4-(4-Bromophenyl)pyridine-2,6-diyl)bis(4,1-phenylene)bis(4-methylbenzenesulfonate) (1g).   M.p. = 227–229 °C, FT-IR (KBr, ν, cm^{-1}): 3114, 1602, 1497, 1368, 1152. ^{1}H NMR (301 MHz, DMSO) δ 8.32 (d, J = 9 Hz, 4H), 8.13 (s, 2H), 7.92 (d, J = 9 Hz, 2H), 7.82 (d, J = 9 Hz, 4H), 7.51 (d, J = 6 Hz, 4H), 7.18 (d, J = 9 Hz, 4H), 6.95 (d, J = 9 Hz, 2H),

2.45 (s, 6H, CH$_3$). ^{13}C NMR (76 MHz, DMSO) δ 159.6, 155.4, 150.2, 150.1, 146.4, 138.3, 131.9, 130.8, 129.2, 129.1, 128.8, 128.1, 122.7, 116.5, 116.3, 21.7.

(4-(4-Isopropylphenyl)pyridine-2,6-diyl)bis(4,1-phenylene)dibenzenesulfonate (2a). M.p. = 145–148 °C, FT-IR (KBr, ν, cm^{-1}): 3069, 2960, 1603, 1503, 1367, 1199. ^{1}H NMR (301 MHz, DMSO) δ 8.33 (d, *J* = 9 Hz, 4H), 8.17 (s, 2H), 7.95 (d, *J* = 9 Hz, 5H), 7.86–7.83 (m, 1H), 7.74–7.69 (m, 4H), 7.43 (d, *J* = 9 Hz, 2H), 7.19 (d, *J* = 8.9 Hz, 4H), 2.98 (hept, *J* = 6 Hz, 1H, CH), 1.26 (d, *J* = 6.9 Hz, 6H, CH$_3$). ^{13}C NMR (76 MHz, DMSO) δ 155.5, 150.4, 150.2, 150.2, 138.2, 135.6, 135.4, 134.8, 130.4, 129.1, 128.7, 127.7, 127.5, 122.8, 117.3, 33.7, 24.2. ESI–MS (m/z) = calcd. for C$_{38}$H$_{31}$NO$_6$S$_2$ (M$^+$) 661.15, found: 662.

(4-(4-Methoxyphenyl)pyridine-2,6-diyl)bis(4,1-phenylene)dibenzenesulfonate (2b). M.p. = 111–113 °C, FT-IR (KBr, ν, cm^{-1}): 3067, 2923, 1599, 1501, 1373, 1178. ^{1}H NMR (301 MHz, DMSO) δ 8.33 (d, *J* = 9 Hz, 4H), 8.17 (s, 2H), 8.03 (d, *J* = 9 Hz, 2H), 7.96–7.93 (m, 4H), 7.89–7.83 (m, 2H), 7.74–7.69 (m, 4H), 7.19 (d, *J* = 9 Hz, 4H), 7.11 (d, *J* = 9 Hz, 2H), 3.86 (s, 3H, OCH$_3$). ^{13}C NMR (76 MHz, DMSO) δ 161.0, 155.5, 150.2, 149.8, 138.3, 135.6, 134.8, 130.4, 129.9, 129.2, 129.1, 128.8, 122.7, 116.8, 114.9, 55.8.

(4-(4-Chlorophenyl)pyridine-2,6-diyl)bis(4,1-phenylene)dibenzenesulfonate (2c). M.p. = 186–189 °C, FT-IR (KBr, ν, cm^{-1}): 3064, 2926, 1606, 1546, 1494, 1371, 1152. ^{1}H NMR (301 MHz, DMSO) δ 8.35 (d, *J* = 9 Hz, 4H), 8.23 (s, 2H), 8.12–8.08 (m, 2H), 7.96–7.93 (m, 4H), 7.91–7.84 (m, 4H), 7.74–7.69 (m, 4H), 7.63 (s, 1H), 7.22–7.18 (m, 4H). ^{13}C NMR (76 MHz, DMSO) δ 155.7, 150.3, 148.9, 138.1, 136.6, 135.6, 134.8, 131.0, 130.8, 130.4, 129.7, 129.5, 129.2, 128.8, 117.4.

(4-(2-Chlorophenyl)pyridine-2,6-diyl)bis(4,1-phenylene)dibenzenesulfonate (2d). M.p. = 125–127 °C, FT-IR (KBr, ν, cm^{-1}): 3061, 2923, 1603, 1504, 1448, 1371, 1152. ^{1}H NMR (301 MHz, DMSO) δ 8.29 (d, *J* = 9 Hz, 4H), 8.01 (s, 2H), 7.95–7.92 (m, 4H), 7.85 (dt, *J* = 9, 1.7 Hz, 2H), 7.73 (d, *J* = 9 Hz, 4H), 7.68–7.65 (m, 2H), 7.55–7.51 (m, 2H), 7.19 (d, *J* = 9 Hz, 4H). ^{13}C NMR (76 MHz, DMSO) δ 155.0, 150.3, 149.3, 137.9, 137.8, 135.6, 134.8, 131.9, 131.7, 130.9, 130.5, 130.4, 129.1, 128.7, 128.2, 122.9, 120.4.

N,N′-((4-Phenylpyridine-2,6-diyl)bis(4,1-phenylene))bis(4-methylbenzenesulfonamide) (3a). M.p. = 114–116 °C, FT-IR (KBr, ν, cm^{-1}): 3259, 2923, 1694, 1603, 1598, 1514, 1331, 1160. ^{1}H NMR (301 MHz, DMSO) δ 10.47 (s, 2H, NH), 8.19 (d, *J* = 9 Hz, 4H), 8.03 (s, 2H), 7.96 (d, *J* = 6 Hz, 2H), 7.76 (d, *J* = 9 Hz, 4H), 7.58–7.50 (m, 2H), 7.37–7.28 (m, 8H), 2.31 (s, 6H, CH$_3$). ^{13}C NMR (76 MHz, DMSO) δ 162.8, 156.2, 149.9, 143.9, 139.4, 138.2, 137.2, 134.6, 130.2, 129.5, 128.3, 127.7, 127.3, 127.2, 120.0, 116.1, 21.4.

N,N′-((4-(4-Chlorophenyl)pyridine-2,6-diyl)bis(4,1-phenylene))bis(4-methylbenzenesulfonamide) (3b). M.p. = 127–129 °C, FT-IR (KBr, ν, cm^{-1}): 3256, 2929, 1600, 1514, 1332, 1160. ^{1}H NMR (301 MHz, DMSO) δ 10.53 (s, 2H, NH), 8.18 (d, *J* = 9 Hz, 4H), 8.05–8.02 (m, 4H), 7.74 (d, *J* = 9 Hz, 4H), 7.61 (d, *J* = 6 Hz, 2H), 7.37 (d, *J* = 6 Hz, 4H), 7.27 (d, *J* = 9 Hz, 4H), 2.33 (s, 6H, CH$_3$). ^{13}C NMR (76 MHz, DMSO) δ 156.2, 148.5, 143.9, 139.4, 137.2, 137.0, 134.7, 134.5, 130.2, 129.6, 129.5, 128.3, 127.3, 119.9, 116.0, 21.4. ESI–MS (m/z) = calcd. for C$_{37}$H$_{30}$ClN$_3$O$_4$S$_2$ (M$^+$) 680.23, found: 680.

N,N′-((4-(4-Bromophenyl)pyridine-2,6-diyl)bis(4,1-phenylene))bis(4-methylbenzenesulfonamide) (3c). M.p. = 143–144 °C, FT-IR (KBr, ν, cm^{-1}): 3250, 2920, 1600, 1514, 1322, 1160. ^{1}H NMR (301 MHz, DMSO) δ 10.54 (s, 2H, NH), 8.18 (d, *J* = 9 Hz, 4H), 8.03 (s, 2H), 7.97–7.92 (m, 2H), 7.75–7.72 (m, 6H), 7.36 (d, *J* = 6 Hz, 4H), 7.28 (d, *J* = 9 Hz, 4H), 2.32 (s, 6H, CH$_3$). ^{13}C NMR (76 MHz, DMSO) δ 155.6, 150.3, 148.7, 146.4, 137.9, 136.8, 131.9, 130.8, 129.6, 129.1, 128.8, 123.1, 122.8, 117.5, 22.2.

(1,4-Phenylenebis(pyridine-4,2,6-triyl))tetrakis(benzene-4,1-diyl)tetrakis(4-methylbenzenesulfonate) (1 h). M.p. ≥ 300 °C, FT-IR (KBr, ν, cm^{-1}): 3058, 2926, 1651, 1600, 1499, 1371, 1152. ^{1}H NMR (301 MHz, DMSO) δ 8.4–8.25 (m, 11H), 7.84–7.76 (m, 10H), 7.54–7.48 (m, 10H), 7.31 (d, *J* = 9 Hz, 2H), 7.23–7.17 (m, 5H), 6.99 (d, *J* = 9 Hz, 2H), 2.45 (m, 12H, CH$_3$). ^{13}C NMR (76 MHz, DMSO) δ 168.8, 155.7, 150.4, 148.1, 146.4, 146.2, 144.5, 138.1, 132.2, 131.9, 130.8, 130.7, 129.9, 129.2, 128.8, 128.6, 128.0, 122.8, 122.2, 117.5, 21.7. ESI–MS (m/z) = calcd. for C$_{68}$H$_{52}$N$_2$O$_{12}$S$_4$ (M$^+$) 1217.41, found: 1218.

N,N′,N″,N‴-((1,4-Phenylenebis(pyridine-4,2,6-triyl))tetrakis(benzene-4,1-diyl))tetrakis(4-methylbenzenesulfonamide) (3d). M.p. ≥ 300 °C, FT-IR (KBr, ν, cm^{-1}): 3458, 2925, 1605, 1545, 1368, 1179. ^{1}H NMR (301 MHz, DMSO) δ 10.56 (s, 4H, NH), 8.14 (d, *J* = 9 Hz, 4H), 7.95 (s, 2H), 7.88–7.83 (m, 4H), 7.76–7.71 (m, 10H), 7.40–7.35 (m, 10H), 7.27–7.21 (m, 10H), 2.35–2.33 (m, 12H, CH$_3$). ^{13}C NMR (76 MHz, DMSO) δ 156.1, 148.9, 144.1, 143.9, 143.0, 139.4, 139.3, 137.2, 137.1, 137.0, 134.6, 133.2, 132.3, 130.3, 130.3, 130.2, 128.6, 128.3, 127.2, 127.2, 120.0, 119.9, 118.3, 115.6, 21.4.

Conclusion

In this work, Fe$_3$O$_4$@SiO$_2$@PCLH-TFA as a novel magnetic nanoparticle with pyridinium bridges was designed, synthesized and characterized with FT-IR, EDX, XRD, SEM, TEM, TG/DTG and VSM. Then, Fe$_3$O$_4$@SiO$_2$@PCLH-TFA was applied in the multicomponent synthesis of a new library of triarylpyridines bearing sulfonate and sulfonamide moieties via a cooperative vinylogous anomeric-based oxidation. According to the obtained results, the reactions were performed under mild conditions and short reaction time, and the synthesis of

molecules show good yields. Furthermore, Fe₃O₄@SiO₂@PCLH-TFA show elegant performance in recovering and reusing test.

References

1. Guan, A., Liu, C., Yang, X. & Dekeyser, M. Application of the intermediate derivatization approach in agrochemical discovery. *Chem. Rev.* **114**, 7079–7107 (2014).
2. Gallou, I. Unsymmetrical ureas. Synthetic methodologies and application in drug design. *Org. Prep. Proced. Int.* **39**, 355–383 (2007).
3. Bigi, F., Maggi, R. & Sartori, G. Selected syntheses of ureas through phosgene substitutes. *Green Chem.* **2**, 140–148 (2000).
4. Vishnyakova, T. P., Golubeva, I. A. & Glebova, E. V. Substituted ureas. Methods of synthesis and applications. *Russ. Chem. Rev.* **54**, 249–261 (1985).
5. Kurt, B. Z., Kandas, N. O., Dag, A., Sonmez, F. & Kucukislamoglu, M. Synthesis and biological evaluation of novel coumarin-chalcone derivatives containing urea moiety as potential anticancer agents. *Arab. J. Chem.* **13**, 1120–1129 (2020).
6. Atashkar, B., Zolfigol, M. A. & Mallakpour, S. Applications of biological urea-based catalysts in chemical processes. *Mol. Catal.* **452**, 192–246 (2018).
7. Babad, H. & Zeiler, A. G. Chemistry of phosgene. *Chem. Rev.* **73**, 75–91 (1973).
8. Eckert, H. & Forster, B. Triphosgene, a crystalline phosgene substitute. *Angew. Chem. Int. Ed. Engl.* **26**, 894–895 (1987).
9. Braunstein, P. & Nobel, D. Transition-metal-mediated reactions of organic isocyanates. *Chem. Rev.* **89**, 1927–1945 (1989).
10. Majer, P. & Randal, R. S. A safe and efficient method for preparation of N, N''-unsymmetrically disubstituted ureas utilizing triphosgene. *J. Org. Chem.* **59**, 1937–1938 (1994).
11. Scialdone, M. A., Shuey, S. W., Soper, P., Hamuro, Y. & Burns, D. M. Phosgenated *p*-nitrophenyl (polystyrene) ketoxime or phoxime resin. A new resin for the solid-phase synthesis of ureas via thermolytic cleavage of oxime-carbamates. *J. Org. Chem.* **63**, 4802–4807 (1998).
12. Koya, S. *et al.* Selective synthesis of eight-membered cyclic ureas by the [6+ 2] cycloaddition reaction of 2-vinylazetidines and electron-deficient isocyanates. *Org. Lett.* **11**, 5438–5441 (2009).
13. Kreve, O., Mutlu, H. & Meier, M. A. R. Sustainable routes to polyurethane precursors. *Green Chem.* **15**, 1431–1455 (2013).
14. Baumann, M. & Baxendale, I. R. An overview of the synthetic routes to the best-selling drugs containing 6-membered hetero-cycles. *Beilstein J. Org. Chem.* **9**, 2265–2319 (2013).
15. Taylor, R. D., MacCoss, M. & Lawson, A. D. G. Rings in drugs: miniperspective. *J. Med. Chem.* **57**, 5859–5845 (2014).
16. Altaf, A. A. *et al.* A review on the medicinal importance of pyridine derivatives. *J. Drug Des. Med. Chem.* **1**, 1–11 (2015).
17. Gujjarappa, R., Vodnala, N. & Malakar, C. C. Recent advances in pyridine-based organocatalysis and its application towards valuable chemical transformations. *ChemistrySelect* **5**, 8745–8758 (2020).
18. De Henry, G. D. novo synthesis of substituted pyridines. *Tetrahedron* **29**, 6043–6061 (2004).
19. Allais, C., Grassot, J. M., Rodriguez, J. & Constantieux, T. Metal-free multicomponent syntheses of pyridines. *Chem. Rev.* **114**, 10829–10868 (2014).
20. Spivey, A. C. & Arseniyadis, S. Nucleophilic catalysis by 4-(dialkylamino) pyridines revisited-the search for optimal reactivity and selectivity. *Angew. Chem. Int. Ed.* **43**, 5436–5441 (2004).
21. Afradi, M., Abbasi Pour, S., Dolat, M. & Yazdani-Elah-Abadi, A. Nanomagnetically modified vitamin B3 (Fe3O4@Niacin): An efficient and reusable green biocatalyst for microwave-assisted rapid synthesis of 2-amino-3-cyanopyridines in aqueous medium. *Appl. Organomet. Chem.* **32**, e103 (2017).
22. Asadbegi, S., Bodaghifard, M. A. & Mobinikhaledi, A. Poly N, N-dimethylaniline-formaldehyde supported on silica-coated magnetic nanoparticles: a novel and retrievable catalyst for green synthesis of 2-amino-3-cyanopyridines. *Res. Chem. Intermed.* **46**, 1629–1643 (2020).
23. Khalifeh, R. & Ghamari, M. A multicomponent synthesis of 2-amino-3-cyanopyridine derivatives catalyzed by heterogeneous and recyclable copper nanoparticles on charcoal. *J. Braz. Chem. Soc.* **27**, 759–768 (2016).
24. Khalili, D. A reusable and metal-free carbocatalyst for the one-pot synthesis of 2-amino-3-cyanopyridines in water. *Tetrahedron Lett.* **57**, 1721–1723 (2016).
25. Tamaddon, F., Ghazi, S. & Noorbala, M. R. Urease-catalyzed synthesis of aminocyanopyridines from urea under fully green conditions. *J. Mol. Catal. B: Enzym.* **127**, 89–92 (2016).
26. Yahyazadeh, A., Abbaspour-Gilandeh, E. & Aghaei-Hashjin, M. Four-component synthesis of 2-amino-3-cyanopyridine deriva-tives catalyzed by Cu@imineZCMNPs as a novel, efficient and simple nanocatalyst under solvent-free conditions. *Catal. Lett.* **148**, 1254–1262 (2018).
27. Bull, J. A., Mousseau, J. J., Pelletier, G. & Charette, A. B. Synthesis of pyridine and dihydropyridine derivatives by regio-and stereoselective addition to *N*-activated pyridines. *Chem. Rev.* **112**, 2642–2713 (2012).
28. Reiersølmoen, A. C. *et al.* Catalytic activity of trans-bis (pyridine) gold complexes. *J. Am. Chem. Soc.* **142**, 6439–6446 (2020).
29. Hsieh, S. Y., Tang, Y., Crotti, S., Stone, E. A. & Miller, S. J. Catalytic enantioselective pyridine N-oxidation. *J. Am. Chem. Soc.* **141**, 18624–18629 (2019).
30. Abendroth, J. M., Bushuyev, O. S., Weiss, P. S. & Barrett, C. J. Controlling motion at the nanoscale: rise of the molecular machines. *ACS Nano* **9**, 7746–7768 (2015).
31. Erbas-Cakmak, S., Leigh, D. A., McTernan, C. T. & Nussbaumer, A. L. artificial molecular machines. *Chem. Rev.* **115**, 10081–10206 (2015).
32. Balzani, V., Credi, A. & Venturi, M. Molecular machines working on surfaces and at interfaces. *ChemPhysChem* **9**, 202–220 (2008).
33. Willand-Charnley, R., Fisher, T. J., Johnson, B. M. & Dussault, P. H. Pyridine is an organocatalyst for the reductive ozonolysis of alkenes. *Org. Lett.* **14**, 2242–2245 (2012).
34. Moosavi-Zare, A. R. *et al.* Synthesis and characterization of acetic acid functionalized poly (4-vinylpyridinium) salt as new catalyst for the synthesis of spiropyran derivatives and their biological activity. *J. Mol. Catal. A Chem.* **425**, 217–228 (2016).
35. Tamaddon, F. & Azadi, D. Synthesis and identification of nicotinium sulfate (3-(1-methylpyrrolidin-2-yl) pyridine: H₂SO₄) from tobacco-extracted nicotine: a protic ionic liquid and biocompatible catalyst for selective acetylation of amines. *J. Mol. Liq.* **255**, 406–412 (2018).
36. Gomha, S. M. & Dawood, K. M. Synthesis and antimicrobial activity of novel 2, 4, 6-trisubstituted pyridines having pyrazole moiety. *J. Heterocycl. Chem.* **54**, 1943–1948 (2017).
37. Trejo-Soto, P. J., Hernández-Campos, A., Romo-Mancillas, A., Medina-Franco, J. L. & Castillo, R. In search of AKT kinase inhibi-tors as anticancer agents: Structure-based design, docking, and molecular dynamics studies of 2, 4, 6-trisubstituted pyridines. *J. Biomol. Struct. Dyn.* **36**, 423–442 (2018).

16

38. Kulangiappar, K., Anbukulandainathan, M. & Raju, T. Nuclear versus side-chain bromination of 4-methoxy toluene by an electrochemical method. *Synth. Commun.* **1**, 2494–2502 (2014).
39. Fang, A. G., Mello, J. V. & Finney, N. S. Structural studies of biarylpyridines fluorophores lead to the identification of promising long wavelength emitters for use in fluorescent chemosensors. *Tetrahedron* **60**, 11075–11087 (2004).
40. Durola, F., Sauvage, J. P. & Wenger, O. S. Sterically non-hindering endocyclic ligands of the bi-isoquinoline family. *Chem. Commun.* **2**, 171–173 (2006).
41. Gopalaiah, K., Rao, D. C., Mahiya, K. & Tiwari, A. Iron-catalyzed aerobic oxidative cleavage and construction of C-N bonds: a facile method for synthesis of 2, 4, 6-trisubstituted pyridines. *Asian J. Org. Chem.* **7**, 1872–1881 (2018).
42. Moosavi-Zare, A. R., Zolfigol, M. A., Farahmand, S., Zare, A. & Pourali, A. R. Synthesis of 2, 4, 6-triarylpyridines using ZrOCl$_2$ under solvent-free conditions. *Synlett* **25**, 193–196 (2014).
43. Ren, Z. H., Zhang, Z. Y., Yang, B. Q., Wang, Y. Y. & Guan, Z. H. Copper-catalyzed coupling of oxime acetates with aldehydes: a new strategy for synthesis of pyridines. *Org. Lett.* **13**, 5394–5397 (2011).
44. Adib, M., Ayashi, N. & Mirzaei, P. An efficient synthesis of 2, 4, 6-triarylpyridines by use of benzyl halides under neat conditions. *Synlett* **27**, 417–421 (2016).
45. Ashraf, M. A., Liu, Z., Li, C. & Zhang, D. Magnetic nanocatalysts in synthesis of xanthenes. *Synth. Commun.* **50**, 3777–3795 (2020).
46. Kazemi, M. Reusable nanomagnetic catalysts in synthesis of imidazole scaffolds. *Synth. Commun.* **50**, 2095–2113 (2020).
47. Lin, Y. *et al.* Magnetic nanoparticles applied in targeted therapy and magnetic resonance imaging: crucial preparation parameters, indispensable pre-treatments, updated research advancements and future perspectives. *J. Mater. Chem. B* **8**, 5973–5991 (2020).
48. Dalpozzo, R. Magnetic nanoparticle supports for asymmetric catalysts. *Green Chem.* **17**, 3671–3686 (2015).
49. Hudson, R., Feng, Y., Varma, R. S. & Moores, A. Bare magnetic nanoparticles: sustainable synthesis and applications in catalytic organic transformations. *Green Chem.* **16**, 4493–4505 (2014).
50. Wu, L., Mendoza-Garcia, A., Li, Q. & Sun, S. Organic phase syntheses of magnetic nanoparticles and their applications. *Chem. Rev.* **116**, 10473–10512 (2016).
51. Shylesh, S., Schnemann, V. & Thiel, W. R. Magnetically separable nanocatalysts: bridges between homogeneous and heterogeneous catalysis. *Angew. Chem. Int. Ed.* **49**, 3428–3459 (2010).
52. Mokhtary, M. Recent advances in catalysts immobilized on magnetic nanoparticles. *J. Iran Chem. Soc.* **13**, 1827–1845 (2016).
53. Karimi, B., Mansouri, F. & Mirzaei, H. M. Recent applications of magnetically recoverable nanocatalysts in C-C and C-X coupling reactions. *ChemCatChem* **7**, 1736–1789 (2015).
54. Maleki, A. Fe$_3$O$_4$/SiO$_2$ nanoparticles: an efficient and magnetically recoverable nanocatalyst for the one-pot multicomponent synthesis of diazepines. *Tetrahedron* **68**, 7827–7833 (2012).
55. Maleki, A., Kari, T. & Aghaei, M. Fe$_3$O$_4$@SiO$_2$@TiO$_2$-OSO $_3$H: an efficient hierarchical nanocatalyst for the organic quinazolines syntheses. *J. Porous Mater.* **24**, 1481–1496 (2017).
56. Maleki, A. One-pot three-component synthesis of pyrido [2′, 1′: 2, 3] imidazo [4, 5-c] isoquinolines using Fe$_3$O$_4$@SiO$_2$–OSO$_3$H as an efficient heterogeneous nanocatalyst. *RSC Adv.* **4**, 64169–64173 (2014).
57. Ulbrich, K. *et al.* Targeted drug delivery with polymers and magnetic nanoparticles: covalent and noncovalent approaches, release control, and clinical studies. *Chem. Rev.* **116**, 5338–5431 (2016).
58. Reddy, L. H., Arias, J. L., Nicolas, J. & Couvreur, P. Magnetic nanoparticles: design and characterization, toxicity and biocompatibility, pharmaceutical and biomedical applications. *Chem. Rev.* **112**, 5818–5878 (2012).
59. Gatteschi, D., Fittipaldi, M., Sangregorio, C. & Sorace, L. Exploring the no-man's land between molecular nanomagnets and magnetic nanoparticles. *Angew. Chem. Int. Ed.* **51**, 4792–4800 (2012).
60. Jun, Y. W., Lee, J. H. & Cheon, J. Chemical design of nanoparticle probes for high-performance magnetic resonance imaging. *Angew. Chem. Int. Ed.* **47**, 5122–5135 (2008).
61. Lu, A. H., Salabas, E. E. & Schüth, F. Magnetic nanoparticles: synthesis, protection, functionalization, and application. *Angew. Chem. Int. Ed.* **46**, 1222–1244 (2007).
62. Ying, A. *et al.* Ionic tagged DABCO grafted on magnetic nanoparticles: a water-compatible catalyst for the aqueous aza-Michael addition of amines to α, β-unsaturated amides. *Catal. Sci. Technol.* **4**, 2115–2125 (2014).
63. Ying, A., Qiu, F., Wu, C., Hu, H. & Yang, J. Ionic tagged amine supported on magnetic nanoparticles: synthesis and application for versatile catalytic Knoevenagel condensation in water. *RSC Adv.* **4**, 33175–33183 (2014).
64. Yarie, M. *et al.* Novel magnetic nanoparticles with ionic liquid tags as a reusable catalyst in the synthesis of polyhydroquinolines. *RSC Adv.* **6**, 82842–82853 (2016).
65. Zolfigol, M. A. & Yarie, M. Synthesis and characterization of novel silica-coated magnetic nanoparticles with tags of ionic liquid. Application in the synthesis of polyhydroquinolines. *RSC Adv.* **5**, 103617–103624 (2015).
66. Zhou, Z. Y., Zhao, W. R., Zhang, J., Chen, X. L. & Tang, J. Y. Sodium tanshinone IIA sulfonate: A review of pharmacological activity and pharmacokinetics. *Biomed. Pharmacother.* **118**, 109362–109373 (2019).
67. Haynes, D. A., Chisholm, J. A., Jones, W. & Motherwell, W. S. Supramolecular synthon competition in organic sulfonates: A CSD survey. *Cryst. Eng. Commun.* **6**, 584–588 (2004).
68. Bouhdada, M., Amane, M. E. & El Hamzaoui, N. Synthesis, spectroscopic studies, X-ray powder diffraction data and antibacterial activity of mixed transition metal complexes with sulfonate azo dye, sulfamate and caffeine ligands. *Inorg. Chem. Commun.* **101**, 32–39 (2019).
69. JinXing, X. Determination of sodium gualenate in L-glutamine and sodium gualenate granules. *Asian Pac. J. Trop. Dis.* **9**, 885–931 (2009).
70. Schwarz, S., Onken, D. & Schubert, A. The steroid story of Jenapharm: From the late 1940s to the early 1970s. *Steroids* **64**, 439–445 (1999).
71. Elgemeie, G. H., Azzam, R. A. & Elsayed, R. E. Sulfa drug analogs: new classes of N-sulfonyl aminated azines and their biological and preclinical importance in medicinal chemistry. *Med. Chem. Res.* **28**, 1099–1131 (2019).
72. Vicente-Blázquez, A. *et al.* Antitubulin sulfonamides: The successful combination of an established drug class and a multifaceted target. *Med. Res. Rev.* **39**, 775–830 (2019).
73. Kang, S. M. *et al.* Inhibition of cancer cell invasion by new ((3, 4-dihydroxy benzylidene) hydrazinyl) pyridine-3-sulfonamide analogs. *Bioorganic Med. Chem. Lett.* **26**, 1322–1328 (2016).
74. Apaydın, S. & Török, M. Sulfonamide derivatives as multi-target agents for complex diseases. Bioorganic and medicinal chemistry letters. *Bioorganic Med. Chem. Lett.* **29**, 2042–2050 (2019).
75. Riaz, S. *et al.* Pyridine sulfonamide as a small key organic molecule for the potential treatment of type-II diabetes mellitus and Alzheimer's disease: in vitro studies against yeast α-glucosidase, acetylcholinesterase and butyrylcholinesterase. *Bioorg. Chem.* **63**, 64–71 (2015).
76. Tian, S. *et al.* Recent progress in sustainable technologies for adsorptive and reactive removal of sulfonamides. *Chem. Eng. J.* **389**, 123423 (2020).
77. Ikaunieks, M., Björkling, F. & Loza, E. The synthesis of some sulfonamides based on 2, 3-dihydro-1 H-pyrrolo [3, 4-c] pyridine. *Chem Heterocycl Compd.* **51**, 658–663 (2015).
78. Li, M., Takada, K., Goldsmith, J. I. & Bernhard, S. Iridium (III) bis-pyridine-2-sulfonamide complexes as efficient and durable catalysts for homogeneous water oxidation. *Inorg. Chem.* **55**, 518–526 (2016).

79. Pour, Z. R., Nazifi, S. M. R., Safavi, A. A., Nazifi, Z. S. & Massah, A. R. Solvent-FREE SYNTHESIS, ADME prediction, and evaluation of antibacterial activity of novel sulfonamide derivatives. *Russ. J. Org. Chem.* **55**, 852–859 (2019).

80. Pinheiro, L. C., Maria de Lourdes, G. F., Silveira, F. F., Feitosa, L. M. & Boechat, N. Antimalarial and anti-inflammatory activities of new chloroquine and primaquine hybrids: Targeting the blockade of malaria parasite transmission. *Med Chem Res.* **28**, 115832 (2019).

81. Erhardt, J. M. & Wuest, J. D. Transfer of hydrogen from orthoamides. Reduction of protons to molecular hydrogen. *J. Am. Chem. Soc.* **102**, 6363–6364 (1980).

82. Juaristi, E. & Cuevas, G. Recent studies of the anomeric effect. *Tetrahedron* **48**, 5019–5087 (1992).

83. Edward, J. T. Stability of glycosides to acid hydrolysis. *Chem. Ind.* **3**, 1102–1104 (1955).

84. Glover, S. A. Anomeric amides—structure, properties and reactivity. *Tetrahedron* **54**, 7229–7271 (1998).

85. Glover, S. A. & Rosser, A. A. HERON reactions of anomeric amides: Understanding the driving force. *J. Phys. Org. Chem.* **28**, 215–222 (2015).

86. Alabugin, I. V. *Stereoelectronic Effects. A Bridge Between Structure and Reactivity* (Wiley, Hoboken, 2016).

87. Alabugin. I. V., Gomes, G, P. & Abdo, M. *WIREs Comput. Mol. Sci.* **9**, e1389 (2019).

88. Alabugin, I. V., Gilmore, K. M. & Peterson, P. W. Hyperconjugation. Wiley interdisciplinary reviews. *WIREs Comput Mol. Sci.* **1**, 109–141 (2011).

89. Vatsadze, S. Z., Loginova, Y. D., dos Passos Gomes, G. & Alabugin, I. V. Stereoelectronic chameleons: the donor–acceptor dichotomy of functional groups. *Chem. Eur. J.* **23**, 3225–3245 (2017).

90. Wilcox, C. F. & Bauer, S. H. DFT calculations of thermochemical and structural parameters of tetracyanohydrazine and related tetrasubstituted hydrazines. *J Mol Struct-Theochem.* **625**, 1–8 (2003).

91. Curran, D. P. & Suh, Y. G. Selective mono-Claisen rearrangement of carbohydrate glycals. A chemical consequence of the vinylogous anomeric effect. *Carbohydr. Res.* **171**, 161–191 (1987).

92. Denmark, S. E., Dappen, M. S., Sear, N. L. & Jacobs, R. T. The vinylogous anomeric effect in 3-alkyl-2-chlorocyclohexanone oximes and oxime ethers. *J. Am. Chem. Soc.* **112**, 3466–3474 (1990).

93. Katritzky, A. R., Steel, P. J. & Denisenko, S. N. X-Ray crystallographic evidence for a vinylogous anomeric effect in benzotriazole-substituted heterocycles. *Tetrahedron* **57**, 3309–3314 (2001).

94. Jäkel, C. & Dötz, K. H. Organotransition metal modified sugars: Part 22. Direct metalation of glycals: short and efficient routes to diversely protected stannylated glycals. *J. Organomet. Chem.* **624**, 172–185 (2001).

95. Drew, M. D., Wall, M. C. & Kim, J. T. Stereoselective propargylation of glycals with allenyltributyltin (IV) via a Ferrier type reaction. *Tetrahedron Lett.* **53**, 2833–2836 (2012).

96. Nowacki, A., Walczak, D. & Liberek, B. Fully acetylated 1, 5-anhydro-2-deoxypent-1-enitols and 1, 5-anhydro-2, 6-dideoxyhex-1-enitols in DFT level theory conformational studies. *Carbohydr. Res.* **352**, 177–185 (2012).

97. Asgari, M. & Nori-Shargh, D. Exploring the impacts of the vinylogous anomeric effect on the synchronous early and late transition states of the hydrogen molecule elimination reactions of cis-3, 6-dihalocyclohexa-1, 4-dienes. *Struct. Chem.* **28**, 1803–1814 (2017).

98. Nowacki, A. & Liberek, B. Acetylated methyl 1, 2-dideoxyhex-1-enopyranuronates in density functional theory conformational studies. *Carbohydr. Res.* **371**, 1–7 (2013).

99. Nowacki, A. & Liberek, B. *Carbohydr. Res.* **462**, 13–27 (2018).

100. Gomez, A. M., Lobo, F., Uriel, C. & Lopez, J. C. *Eur. J. Org. Chem.* **32**, 7221–7262 (2013).

101. Karimi, F., Yarie, M. & Zolfigol, M. A. Synthesis and characterization of $Fe_3O_4@SiO_2@(CH_2)_3NH(CH_2)_2O_2P(OH)_2$ and its catalytic application in the synthesis of benzo-[*h*] quinoline-4-carboxylic acids via a cooperative anomeric based oxidation mechanism. *Mol. Catal.* **489**, 110924–110933 (2020).

102. Karimi, F., Yarie, M. & Zolfigol, M. A. $Fe_3O_4@SiO_2@(CH_2)_3$-urea-thiourea: A novel hydrogen-bonding and reusable catalyst for the construction of bipyridine-5-carbonitriles via a cooperative vinylogous anomeric based oxidation. *Mol. Catal.* **497**, 111201 (2020).

103. Ghasemi, P., Yarie, M., Zolfigol, M. A., Taherpour, A. & Torabi, M. Ionically tagged magnetic nanoparticles with urea linkers: application for preparation of 2-aryl-quinoline-4-carboxylic acids via an anomeric-based oxidation mechanism. *ACS Omega* **5**, 3207–3217 (2020).

104. Karimi, F., Yarie, M. & Zolfigol, M. A. A convenient method for synthesis of terpyridines via a cooperative vinylogous anomeric based oxidation. *RSC Adv.* **10**, 25828–25835 (2020).

105. Dashteh, M. *et al.* Synthesis of cobalt tetra-2, 3-pyridiniumporphyrazinato with sulfonic acid tags as an efficient catalyst and its application for the synthesis of bicyclic ortho-aminocarbonitriles, cyclohexa-1, 3-dienamines and 2-amino-3-cyanopyridines. *RSC Adv.* **10**, 27824–27834 (2020).

106. Karimi, F., Yarie, M. & Zolfigol, M. A. A novel and reusable ionically tagged nanomagnetic catalyst: Application for the preparation of 2-amino-6-(2-oxo-2*H*-chromen-3-yl)-4-arylnicotinonitriles via vinylogous anomeric based oxidation. *Mol. Catal.* **463**, 20–29 (2019).

107. Torabi, M. *et al.* Synthesis of new pyridines with sulfonamide moiety via a cooperative vinylogous anomeric-based oxidation mechanism in the presence of a novel quinoline-based dendrimer-like ionic liquid. *RSC Adv.* **11**, 3143–3152 (2021).

108. Yarie, M. Catalytic anomeric based oxidation. *Iran. J. Catal.* **7**, 85–88 (2017).

109. Yarie, M. Catalytic vinylogous anomeric based oxidation (Part I). *Iran. J. Catal.* **10**, 79–83 (2020).

110. Afsar, J. *et al.* Synthesis and application of melamine-based nano catalyst with phosphonic acid tags in the synthesis of (3′-indolyl) pyrazolo [3, 4-b] pyridines via vinylogous anomeric based oxidation. *Mol. Catal.* **482**, 110666 (2020).

111. Babaee, S., Zarei, M., Sepehrmansourie, H., Zolfigol, M. A. & Rostamnia, S. Synthesis of metal–organic frameworks MIL-101 (Cr)-NH₂ containing phosphorous acid functional groups: Application for the synthesis of *N*-Amino-2-pyridone and pyrano [2, 3-c] pyrazole derivatives via a cooperative vinylogous anomeric-based oxidation. *ACS Omega* **5**, 6240–6249 (2020).

112. Jalili, F., Zarei, M., Zolfigol, M. A., Rostamnia, S. & Moosavi-Zare, A. R. SBA-15/PrN $(CH_2PO_3H_2)_2$ as a novel and efficient mesoporous solid acid catalyst with phosphorous acid tags and its application on the synthesis of new pyrimido [4, 5-*b*] quinolones and pyrido [2, 3-*d*] pyrimidines via anomeric based oxidation. *Microporous Mesoporous Mater.* **294**, 109865 (2020).

113. Zolfigol, M. A. Silica sulfuric acid/$NaNO_2$ as a novel heterogeneous system for production of thionitrites and disulfides under mild conditions. *Tetrahedron* **57**, 9509–9511 (2001).

114. X-ray data for VI: $C_{11}H_{18}N_4O_3S$, M = 286.35, monoclinic system, space group $C2/c$, a = 12.140(2), b = 10.907(2), c = 11.096(2) Å; β = 96.35(3)º; V = 1460.2(5) Å³, Z = 4, Dcalcd = 1.303 g cm⁻³, μ(Mo-Kα)= 0.232 mm⁻¹, crystal dimension of 0.35×0.25×0.2 mm. The X-ray diffraction measurement was made on a STOE IPDS 2T diffractometer with graphite monochromated Mo-Kα radiation. The structure was solved by using SHELXS. The Data reduction and structure refinement was carried out with SHELXL using the X-STEP32 crystallographic software package. The non-hydrogen atoms were refined anisotropically by full matrix least-squares on F^2 values to final R_1 = 0.0751, wR_2 = 0.1549 and S = 1.053 with 95 parameters using 1967 independent reflection (θ range = 2.52–29.27°). Hydrogen atoms were added in idealized positions. The crystallographic information file has been deposited with the Cambridge Data Centre, CCDC 2062717.

115. *X-STEP32 Version 1.07b, Crystallographic Package*; Stoe & Cie GmbH: Darmstadt, Germany, 2000.

116. Bisenieks, E., Uldrikis, J. & Duburs, G. Reaction of 3, 5-carbonyl-substituted 1, 4-dihydropyridines with hydrazine hydrate. *Chem Heterocycl Compd.* **40**, 869–875 (2004).

117. Schneider, L. M. *et al.* Asymmetric synthesis of carbocyclic propellanes. *Org. Lett.* **19**, 2310–2313 (2017).
118. Wang, X. *et al.* Convenient synthesis of 3, 5-biscarbamoyl-pyridine derivatives. *Chin. J. Chem.* **29**, 2119–2123 (2011).
119. Qu, S. *et al.* Magnetite nanoparticles prepared by precipitation from partially reduced ferric chloride aqueous solutions. *J. Colloid Interf. Sci.* **215**, 190–192 (1999).
120. Lei, X., Jalla, A., Abou Shama, M. A., Stafford, J. M. & Cao, B. Chromatography-free and eco-friendly synthesis of aryl tosylates and mesylates. *Synthesis* **47**, 2578–2585 (2015).
121. Kim, E. J. *et al.* Chemoselective regulation of TREK2 channel: Activation by sulfonate chalcones and inhibition by sulfonamide chalcones. *Bioorg. Med. Chem. Lett.* **20**, 4237–4239 (2010).

Acknowledgements

Author contributions

M.T.: Methodology, investigation, writing—original draft. M.A.Z.: Supervision, resources, project administration, funding acquisition, conceptualization, writing—review and editing. M.Y.: Methodology, investigation, writing—original draft. B.N: Writing—X-ray data. S.A., Kinetic design and study, Project administration, Writing—review and editing. M.M.A., Kinetic Investigation.

Competing interests

The authors declare no competing interests.

Additional information

Supplementary Information The online version contains supplementary material available at https://doi.org/10.1038/s41598-021-95830-w.

Correspondence and requests for materials should be addressed to M.A.Z.

Reprints and permissions information is available at www.nature.com/reprints.

Publisher's note Springer Nature remains neutral with regard to jurisdictional claims in published maps and institutional affiliations.